Journal of Geophysical Research: Atmospheres

RESEARCH ARTICLE
10.1029/2018JD028470

Precipitation Origins and Key Drivers of Precipitation Isotope (^{18}O, ^{2}H, and ^{17}O) Compositions Over Windhoek

Kudzai Farai Kaseke[1], Lixin Wang[1], Heike Wanke[2], Chao Tian[1], Matthew Lanning[1], and Wenzhe Jiao[1]

[1]Department of Earth Sciences, Indiana University-Purdue University Indianapolis, Indianapolis, IN, USA, [2]Geology Department, University of Namibia, Windhoek, Namibia

Key Points:
- The influences of subtropical Atlantic Ocean moisture on southern African precipitation are nonnegligible, especially during droughts
- Precipitation isotopes can identify drought mechanisms, for example, synoptic-scale (El Niño) versus mesoscale drought
- Precipitation $\delta^{18}O$, $\delta^{2}H$, and $\delta^{17}O$ are independent of precipitation type (stratiform versus convective) in the study area

Supporting Information:
- Supporting Information S1
- Data Set S1

Correspondence to:
L. Wang,
lxwang@iupui.edu

Citation:
Kaseke, K. F., Wang, L., Wanke, H., Tian, C., Lanning, M., & Jiao, W. (2018). Precipitation origins and key drivers of precipitation isotope (^{18}O, ^{2}H, and ^{17}O) compositions over Windhoek. *Journal of Geophysical Research: Atmospheres*, *123*. https://doi.org/10.1029/2018JD028470

Received 1 FEB 2018
Accepted 30 JUN 2018
Accepted article online 6 JUL 2018

Abstract Southern African climate is characterized by large precipitation variability, and model precipitation estimates can vary by 70% during summer. This may be partly attributed to underestimation and lack of knowledge of the exact influence of the Atlantic Ocean on precipitation over the region. The current study models trajectories of precipitation events sampled from Windhoek (2012–2016), coupled with isotopes ($\delta^{18}O$, $\delta^{2}H$, $\delta^{17}O$, *d*, and $\delta'^{17}O$-$\delta'^{18}O$) to determine key local drivers of isotope compositions as well as infer source evaporative conditions. Multiple linear regression analyses suggest that key drivers of isotope compositions (relative humidity, precipitation amount, and air temperature) account for 47–53% of $\delta^{18}O$, $\delta^{2}H$, and $\delta^{17}O$ variability. Surprisingly, precipitation $\delta^{18}O$, $\delta^{2}H$, and $\delta^{17}O$ were independent of precipitation type (stratiform versus convective), and this may be attributed to greater modification of stratiform compared to convective raindrops, leading to convergence of isotopes from these precipitation types. Trajectory analyses showed that 78% and 21% of precipitation events during the period originated from the Indian and South Atlantic Oceans, respectively. Although precipitation from the Atlantic Ocean was significantly enriched compared to that from the Indian Ocean ($p < 0.05$), *d* was similar, suggesting significant local modification (up to 55% of *d* variability). Therefore, *d* may not be a conservative tracer of evaporation conditions at the source, at least for Windhoek. The $\delta'^{17}O$-$\delta'^{18}O$ appeared to be a better alternative to *d*, consistent with trajectory analyses, and appeared to differentiate El Niño from non-El Niño droughts. Thus, $\delta'^{17}O$-$\delta'^{18}O$ could be a novel tool to identify drought mechanisms.

1. Introduction

The climate of southern Africa, defined as the land area bound by the region 15–35°S; 12.5–42.5°E, is complex and involves the interaction of several factors that alternate in importance (Allan et al., 2003; Reason & Rouault, 2002; Richard et al., 2000). Traditionally, Atlantic influences on southern African precipitation have been downplayed, and this could be attributed to data paucity, lack of awareness of the complexities of the atmosphere-ocean coupling and associated tropical-extratropical interactions, and perceptions that Atlantic influences were secondary to those from the Indian or Pacific Oceans (El Niño–Southern Oscillation, ENSO; Reason et al., 2006). Therefore, precipitation over southern Africa has been associated with sea surface temperatures (SSTs) from the Indian Ocean (D'Abreton & Lindesay, 1993; Reason & Mulenga, 1999). However, there is growing consensus that the South Atlantic Ocean may play a significant role on climate in the region, although the exact influences are unknown (Reason et al., 2006). Given this uncertainty in moisture origins, it is not surprising that model estimates of precipitation over the region vary depending on a model's representation of the Angola Low, a regional circulation feature which can account for as much as 60% of the intermodel variability (Munday & Washington, 2017). The ability to capture this ocean-atmospheric circulation feature might drive the disagreement between models. Therefore, despite the tight coupling between precipitation and society in southern Africa (Conway et al., 2015), our knowledge of precipitation patterns and their climate controls for the region are limited (Reason et al., 2006).

Stable isotopes of hydrogen and oxygen ($\delta^{2}H$ and $\delta^{18}O$) are unique environmental tracers that can be used to understand dynamics and processes in hydrology, geology, ecology, and climate research (Gat, 1996; Stumpp et al., 2014; Zhao et al., 2012). However, relatively few studies across Africa have applied stable isotopes of precipitation to climate research. Although global isoscapes reproduce reasonably well the global distribution of mean annual isotope contents of modern precipitation (Risi et al., 2010; Werner et al., 2011), they do not explain observed seasonal or interannual variations at a regional or local scale (Field, 2010; Lee et al., 2007;

Risi et al., 2010; Schmidt et al., 2005; Vuille et al., 2003) and do not downscale well in data scarce regions (Kaseke et al., 2016; Terzer et al., 2013). Furthermore, multiscale influences on the isotopic composition of precipitation do not conform well to univariate regression analysis in midlatitude and subtropical locations (Alley & Cuffey, 2001; Fricke & O'Neil, 1999; Sturm et al., 2010). In addition, event-scale studies capture day-to-day synoptic variation that may be lost or diluted in monthly samples (Liu et al., 2010; Noone & Simmonds, 2002). Therefore, event-scale comparisons with aggregated data may help define underlying uncertainties in relationships between the isotopic composition of precipitation and climate variables (Soderberg et al., 2013).

The moisture that eventually becomes precipitation is derived primarily from the oceans and/or evapotranspiration from the terrestrial surface (Sjostrom & Welker, 2009). Therefore, traditional approaches have suggested that air mass history may influence the isotopic composition of precipitation (Dansgaard, 1964). In addition to δ^2H and $\delta^{18}O$, *d*-excess defined as $d = \delta^2H - 8 \times \delta^{18}O$ (Dansgaard, 1964) has been used to determine evaporative conditions (Merlivat & Jouzel, 1979). However, recent work suggests that *d* may not be a true conservative tracer of evaporation conditions (Lai & Ehleringer, 2011; Welp et al., 2012; Zhao et al., 2014). Until recently, it was assumed that $\delta^{17}O$ in precipitation did not carry any additional information to that of $\delta^{18}O$ (Angert et al., 2004). However, recent work indicates that $\delta^{17}O$-$\delta^{18}O$ is independent of temperature and can be used to differentiate fractionation processes (Angert et al., 2004; Kaseke et al., 2017). Therefore, $\delta^{17}O$-excess ($^{17}\Delta$), $^{17}\Delta = \delta'^{17}O - 0.528 \times \delta'^{18}O$, could be a conservative tracer of humidity changes at the vapor source origin and complement $\delta^{18}O$, δ^2H, and *d* (Angert et al., 2004; Barkan & Luz, 2007; Tian et al., 2018). In addition, air mass trajectories have been used to explain precipitation isotope variations in North America (Burnett et al., 2004; Sinclair et al., 2011; Sjostrom & Welker, 2009), Europe (Baldini et al., 2010; Gat & Carmi, 1970), Asia (Fudeyasu et al., 2011; Liu et al., 2011), Australia (Barras & Simmonds, 2008, 2009), and Africa (Lewis et al., 2010; Soderberg et al., 2013). However, despite the complexities of southern African climate, we are not aware of any studies that have investigated the influence of atmospheric trajectories on southern African precipitation isotope compositions. We are also not aware of any studies that have reported $\delta^{17}O$ values in precipitation for the region. Using a 4-year (2012–2016) precipitation data set, the objectives of this study were, thus, to determine storm-to-storm isotopic variability and composition ($\delta^{18}O$, δ^2H, and $\delta^{17}O$) of precipitation in Windhoek (Namibia), identify the local controls of precipitation isotopes, and apply trajectory analysis to determine vapor source origins and $\delta'^{17}O$-$\delta'^{18}O$ relationships to infer evaporation conditions at the source region. The observation period covered three drought years of which two occurred during the 2014–2016 ENSO event. This provided the opportunity to test whether novel $\delta'^{17}O$-$\delta'^{18}O$ techniques could be used to differentiate different types of droughts. We are not aware of any isotope studies that have done this, although a few have focused exclusively on isotope compositions and variability during ENSO events (Sánchez-Murillo et al., 2017).

2. Materials and Methods

2.1. Site Description and Sample Collection

Namibia is located on the southwestern tip of the African continent, and the study site (22.6137°S and 17.09753°E, elevation 1,720 m above sea level) is located in the capital, Windhoek (3,133km^2; Figure 1a). According to the Köppen Climate classification system, Windhoek is a hot semiarid climate (*BSh*) characterized by hot wet summers and cool dry winters. Based on data from the Southern Africa Science Service Centre for Climate Change and Adaptive Land-use (SASSCAL) Windhoek weather station (22.5706°S and 17.0957°E, elevation 1,722 m above sea level), 2012–2016 had the following monthly meteorological characteristics: temperature range (−0.2–36.3 °C), average temperature (20.7 °C), relative humidity (RH) range (0.4–99.6%), and average RH (29.5%; Figures 1b and 1c). Because precipitation is highly seasonal and precipitation events are concentrated between October and April (Lu et al., 2016; Sturm et al., 2009), our analyses were based on the hydrologic year (October to September). Windhoek has not experienced any significant changes in precipitation intensity, frequency, or total amount between 1998 and 2015 (Lu et al., 2016), and because the current study falls within this time frame, results should be comparable to this relatively long-term study.

A total of 109 discrete precipitation events were sampled during the observation period (supporting information Data Set S1). These precipitation events were matched based on the date of sampling to the SASSCAL weather data, which showed 138 events during this period. This total excluded 42 precipitation events recorded by the SASSCAL weather station because there were less than 0.2 mm/day and may have

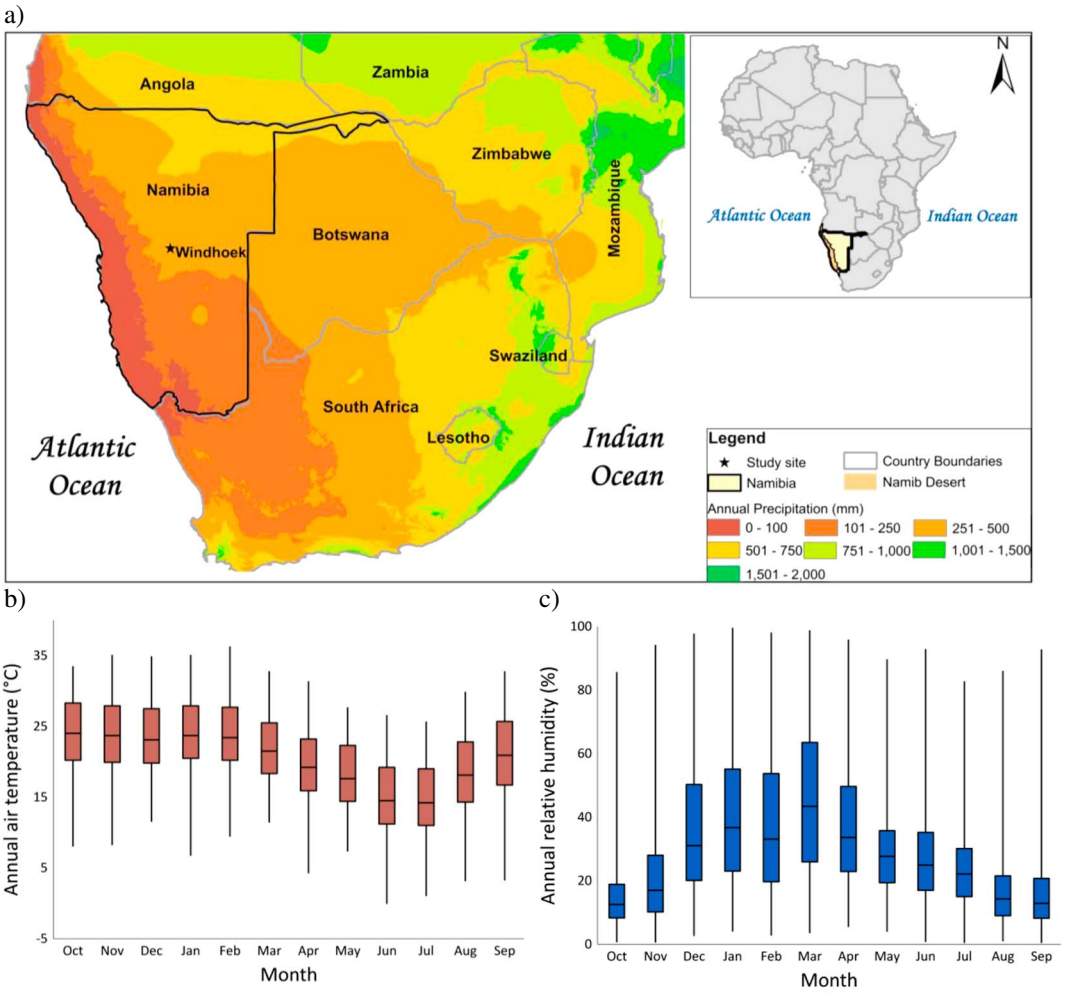

Figure 1. (a) Map showing regional mean annual precipitation (http://www.worldclim.org/bioclim), location of the study site, and Namibia (insert), (b) monthly temperature, and (c) monthly relative humidity for Windhoek (2012–2016). Median represented by dark line in box, while box represents first and third quartile range. Whiskers indicate the maximum and minimum values per month.

resulted in either insufficient sample for analyses or were localized events that did not occur at the sampling site. When possible, samples were collected immediately after the event or the next morning from a manual rain gauge and transferred into 15 ml Qorpak clear French square bottles with black phenolic polycone lined caps. The bottles were labeled with the appropriate site name, date, and amount and stored at 5 °C at the University of Namibia Windhoek campus. Samples were stored for about 6 months and either shipped or retrieved during field campaigns and transported to Indiana University-Purdue University Indianapolis Ecohydrology lab for isotope analysis.

2.2. Isotope Analysis

Isotope analysis was performed using the Triple Water Vapor Analyzer coupled to the Water Vapor Isotope Standard Source (Los Gatos Research Inc., Mountain View, CA, United States) with a reported precision of 0.2‰ $\delta^{18}O$, 0.8‰ $\delta^{2}H$, and 0.4‰ $\delta^{17}O$ similar to those reported elsewhere (Tian et al., 2016; Wang et al., 2009). Data were reported in δ notation relative to Vienna standard mean ocean water (VSMOW)-SLAP scale as

$$\delta = \left(\frac{R_{\text{sample}}}{R_{\text{VSMOW}}} - 1\right) \times 10^3, \tag{1}$$

where R_{sample} and R_{VSMOW} are the molar ratios of heavy to light isotopes ($^{2}H/H$, $^{18}O/^{16}O$, or $^{17}O/^{16}O$) of the sample and international standard—VSMOW. However, it has been demonstrated that when dealing with

high precision ratios in multiple systems, a modified δ is preferred (Hulston & Thode, 1965; Luz & Barkan, 2005; Miller, 2002), hereafter designated as δ' and defined as

$$\delta'^{*}O = \ln(\delta + 1) = \ln\left(\frac{R_{\text{sample}}}{R_{\text{VSMOW}}}\right), \tag{2}$$

where $*O$ is either ^{17}O or ^{18}O.

We computed mean annual isotopic composition as arithmetic and weighted means, adapted from Kazmierz Rozanski and Gonftanttni (1993):

$$\delta\text{Annual weighted} = \Sigma_{\text{September}}^{\text{October}}\delta\text{Event}\, X \frac{ppt_{(\text{Event})}}{ppt_{(\text{Annual Total})}}, \tag{3}$$

where $ppt_{(\text{Event})}$ is the event precipitation amount and $ppt_{(\text{Annual Total})}$ is the annual total precipitation amount as defined by the hydrologic year.

2.3. Local Meteoric Water Lines

Multiple statistical methods have been proposed to calculate the local meteoric water line (LMWL; Crawford et al., 2014). These methods include the unweighted and precipitation weighted versions of the ordinary least squares (OLSR), reduced major axis (RMA), and major axis (MA) regression models. However, because each method has its merits, we present all versions generated from the LMWL Freeware program (Crawford et al., 2014), based on event samples (Table S1). A long-term LMWL (2012–2016) was calculated and used as a reference for the site for comparisons to annual LMWLs from the same period. For statistical comparisons, the unweighted OLSR LMWL (annual and interannual) was adopted to perform the analysis of covariance (ANCOVA). Similarly, annual $\delta'^{17}O$-$\delta'^{18}O$ lines were calculated based on the unweighted OLSR to complement interpretation of the $\delta^{18}O$-$\delta^{2}H$ LMWLs.

2.4. Precipitation Classification: Stratiform Versus Convective

Tropical Rainfall Measuring Mission (TRMM) 2A25 V7 and Global Precipitation Measurement (GPM) 2AKu band satellite data products covering the study area during 2012–2016 were downloaded and analyzed. Because the sampling site was located roughly in the center of Windhoek, the sampling site was taken as the center of a 0.5° × 0.5° square centroid (3,025 km^2) for data retrieval. The level 2 data products of TRMM and GPM have a temporal resolution of 16 orbits a day, and a total of 24 satellite products showed precipitation over the area that corresponded to the Windhoek SASSCAL weather station. Data from both TRMM and GPM classify precipitation into three types: stratiform, convective, and other. However, the third precipitation type *other* was not encountered during our analyses, and according to Aggarwal et al. (2016), it exists at higher levels and may not contribute significantly to precipitation near the surface. Therefore, for the purposes of this study, we excluded the third classification. Average conditional precipitation rates were calculated for each event based on conditional stratiform and convective precipitation rates over the area. The stratiform fraction was defined as the ratio of stratiform rainfall to total conditional precipitation rates. Therefore, stratiform fraction as applied to this paper translates to 0% stratiform = 100% convective except during nonprecipitation days and vice versa.

2.5. Trajectory Analyses

Analysis of discrete precipitation events permits the use of back trajectory models to determine source origins and inference of source evaporation conditions that may influence the isotopic composition of precipitation when coupled with secondary parameters such as *d*. We assumed similar meteorological conditions between the site and the National Botanic Research Institute (NBRI) Windhoek, located 5 km away. This enabled the use of hourly meteorological data from the SASSCAL weather station located at the NBRI. Using this approach, 99 of the 109 precipitation events (91%) at the site were consistent with NBRI data, sampling dates, and general volumes, providing an approximation of local meteorological conditions. The associated meteorological data and event times were then used to calculate the approximate cloud base height of each individual storm based on the lifted condensation level (LCL; Lawrence, 2005; Romps, 2017):

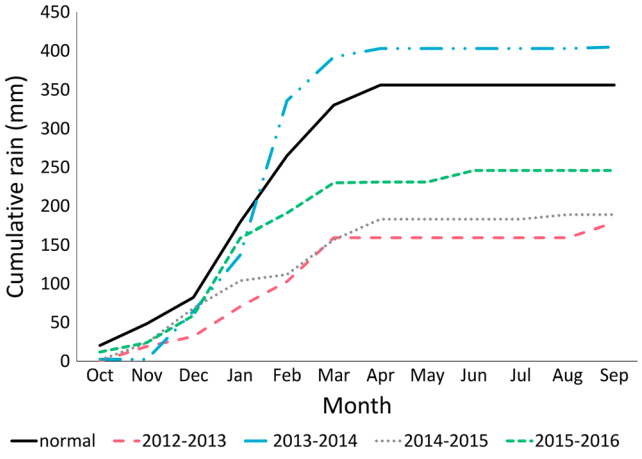

Figure 2. Annual cumulative precipitation totals measured from the site for Windhoek 2012–2016 (October–September) compared to long-term average *normal* precipitation from the Namibia Meteorological Services.

$$LCL = z + \left(20 + \frac{T - 273.15}{5}\right)(100)(1 - RH), \quad (4)$$

where *LCL* is the cloud base height in meters, *T* is absolute temperature, *RH* is relative humidity ranging between 0 and 1, and *z* is the height where *RH* and *T* were measured.

Using LCL to determine the parcels origin height (n = 99), 10-day air mass back trajectories were computed using the Hybrid Single-Particle Lagrangian Integrated Trajectory (HYSPLIT) model (Stein et al., 2015) and meteorological data from the Global Data Assimilation System 1. Because LCL ranged between 83 and 2,154 m above ground level, no trajectories were disqualified for reaching the top of the atmosphere. Global estimates for mean atmospheric moisture residence times range from 4 to 9 days (Läderach & Sodemann, 2016; Trenberth, 1998), while Miralles et al. (2016) estimate an optimal 6-day residence time for the Kalahari ecoregion. The average time for each trajectory from land intersection to Windhoek was about 140 hr (~6 days); thus, trajectory cluster analysis time was set at 140 hr at 6-hr intervals. The total spatial variance for this process was 30%, indicating there was no forcing and misclassification of cluster trajectories (Stein et al., 2015). Trajectory analyses in this study were used primarily to provide the spatial history of an air parcel.

2.6. Statistical Analyses

Statistical analyses were performed in PAST 3 (Hammer et al., 2001) with parametric methods for normally distributed data and nonparametric methods for nonnormally distributed data. Multiple linear regression analyses were performed in XLSTAT 2017 v 4, while trajectory cluster analysis was performed in HYSPLIT (Stein et al., 2015). All data pertaining to this study are provided as Data Set S1.

3. Results and Discussion

3.1. Precipitation Anomalies

Three of the 4 years under observation received below normal precipitation amounts and were classified as meteorological droughts, with the exception of 2013–2014 (Figure 2 and Table S2). Based on the Oceanic Niño Index (ONI; Climate Prediction Center, 2016), two of the three drought years (2014–2015 and 2015–2016) occurred during weak and strong El Niño years, respectively (Figure S1). Given the well-documented effects of ENSO on southern African precipitation (i.e., decrease in precipitation amount; Allan et al., 2003; Nicholson & Entekhabi, 1986; Reason & Rouault, 2002), the 2014–2015 and 2015–2016 meteorological droughts could be El Niño related. However, the 2012–2013 meteorological drought occurred during an El Niño neutral year suggesting that the cause of this drought was different from that of the 2014–2016 droughts (Figure 2, Table S2, and Figure S1). Precipitation was highly seasonal over the sampling period with 89.4–99.5% of annual precipitation occurring during the rainy season, October–April (Table S3). About 55% of the annual precipitation in Windhoek occurs between February–April (late summer), with peak rainfall amounts and largest interannual variability occurring in February (Lu et al., 2016). However, according to the data presented here, with the exception of 2013–2014, less than 50% of annual precipitation occurred during late summer, suggesting droughts resulted in precipitation distribution anomalies over the area (Table S3). Consequently, peak rainfall amounts differed among the years: March for 2012–2013, February for 2013–2014, and January for 2014–2015 and 2015–2016. Interestingly, most precipitation during 2012–2013 occurred during late summer, while for 2014–2015 and 2015–2016, this occurred during early summer (October–January; Table S3). This difference in precipitation distribution among the drought years also suggests that the causes of these droughts, 2012–2013 and 2014–2016, were different, with the 2012–2013 drought being the most severe (Figure 2 and Table S2).

3.2. Precipitation Isotope ($\delta^{18}O$, $\delta^{2}H$, and $\delta^{17}O$) Variations

The long-term *2012–2016* weighted precipitation isotope compositions from this study (Table 1) were comparable to those from Kazmierz Rozanski and Gonftanttni (1993; $\delta^{18}O$-5.0‰) and the Online Isotopes in

Table 1
Annual Weighted and Arithmetic Mean Isotope ($\delta^{18}O$, $\delta^{2}H$, and $\delta^{17}O$) Compositions of Windhoek Precipitation (2012–2016) Based on the Hydrologic Year, October–September

		Mean $\delta^{18}O$‰			Mean $\delta^{2}H$‰			Mean $\delta^{17}O$‰			Mean *d*‰	
Period	*n*	Arith.	WA	Range	Arith.	WA	Range	Arith.	WA	Range	Arith.	Range
2012–2013	26	+0.94	−1.83	−9.74–+7.36	+9.51	−7.55	−60.11 to +57.36	+0.48	−0.96	−5.36 to +4.03	+2.0	−18.9 to +18.6
2013–2014	37	−5.97	−9.03	−15.84–+8.30	−42.44	−63.99	−122.19 to +51.98	−3.14	−4.76	−8.24 to +4.12	+5.3	−17.3 to +15.4
2014–2015	19	−0.41	−3.19	−9.80–+9.31	+1.73	−15.48	−71.10 to +56.00	−0.33	−1.76	−5.38 to +4.69	+5.0	−36.2 to +19.8
2015–2016	27	−1.13	−2.83	−12.39–+7.92	−5.36	−14.39	−85.29 to +48.21	−0.61	−1.46	−6.43 to +4.10	+3.6	−32.3 to +14.9
2012–2016	109	−2.15	−5.17	−15.84–+9.31	−13.16	−33.00	−122.19 to +57.36	−1.16	−2.73	−8.24 to +4.69	+4.0	−36.2 to +19.8

Note. Arith. = arithmetic mean; WA = weighted average.

Precipitation Calculator ($\delta^{18}O$-5.2‰ and $\delta^{2}H$-27.0‰; Bowen, 2017; Bowen & Revenaugh, 2003). Similarly, the unweighted precipitation isotope compositions were comparable to those extracted from the Namibia precipitation isoscape ($\delta^{18}O$-2.9‰ and $\delta^{2}H$-12.6‰; Kaseke et al., 2016) and Kazmierz Rozanski and Gonftanttni (1993; $\delta^{18}O$-2.7‰; Table 1). Therefore, the precipitation isotope results presented in this study are consistent with long-term data presented elsewhere; thus, comparisons of event scale with aggregated data may help define underlying uncertainties between isotopic compositions and climatic variables at longer time scales (Soderberg et al., 2013).

Storm-to-storm isotopic variability over the 4-year period, $\delta^{18}O$ 25‰, $\delta^{2}H$ 180‰, and $\delta^{17}O$ 13‰, was similar to that reported elsewhere (Benson & Klieforth, 1989; Friedman et al., 2002; Liu et al., 2010; Table 1). However, at annual scales, storm-to-storm isotopic variation was lower for the meteorological drought years, while those for the *normal year*, 2013–2014 was similar to the 4-year overall isotopic variability (Table 1). The 2013–2014 precipitation was significantly depleted in $\delta^{18}O$, $\delta^{2}H$, and $\delta^{17}O$ (−5.97‰, −42.44‰, −3.14‰) compared to 2012–2013 (+0.94‰, +9.51‰, +0.48‰), 2014–2015 (−0.41‰, +1.73‰, −0.33‰), and 2015–2016 (−1.13‰, −5.36‰, −0.61‰; one-way analysis of variance, $p < 0.05$; Tukey's post hoc test, $p < 0.05$; Table 1). This could be attributed to the *amount effect* (Dansgaard, 1964), as both annual weighted and arithmetic mean precipitation isotope ($\delta^{18}O$, $\delta^{2}H$, and $\delta^{17}O$) values were significantly inversely related to precipitation amount ($p < 0.05$, Figure S2). One aspect of the amount effect that could be important is subcloud evaporation (Salamalikis et al., 2016). In theory, drought conditions should enhance subcloud evaporation resulting in precipitation enrichment ($\delta^{18}O$, $\delta^{2}H$, and $\delta^{17}O$), lower ranges, and lower *d* compared to normal years (Table 1). However, *d* was similar among the years (Kruskal-Wallis, $p > 0.05$; Table 1) and also similar between the normal (+7.5‰) and drought years (+7.1‰; Mann-Whitney Pairwise test, $p > 0.05$), suggesting that the degree of subcloud evaporation during droughts and normal years at this semiarid site may not differ significantly.

Theoretically, longer travel times would allow for more equilibration time of raindrops with subcloud vapor (isotopic exchange) and subcloud evaporation resulting in higher $\delta^{18}O$, $\delta^{2}H$, and $\delta^{17}O$ values and lower *d* (Table 1). As expected, the median LCL for precipitation events during 2013–2014 (361 m) was significantly lower than that of the drought years (580 m; Mann-Whitney U, $p < 0.005$), indicating longer raindrop travel times from cloud base to the ground surface during droughts. To evaluate the degree of aridity effects between normal and drought years, *d* of drought and normal year precipitation events with LCL between 300 and 600 m (based on the median LCL) was evaluated. The *d* of drought year precipitation events (+10.2‰, range: −8.3‰ to +18.6‰) was significantly larger than for the normal year (+6.8‰, range: −5.2‰ to +15.4‰; Mann-Whitney Pairwise test, $p < 0.05$), suggesting that some other mechanism maybe influencing *d* within this bin and this could be attributed to enhanced moisture recycling during droughts in the Kalahari ecoregion. Although the Kalahari ecoregion experiences a volumetric decrease in precipitation during droughts, it is accompanied by an increase in the recycling ratio (28% versus 34% during wet and drought years), defined as the terrestrially derived precipitation divided by the total precipitation (Miralles et al., 2016). In the Amazon Basin, evaporation (*E*) accounts for about 40% of the evapotranspiration (*ET*) flux and the resultant precipitation is characterized by $d > +10$‰, suggesting a significant part was derived from evaporation (Gat & Matsui, 1991; Martinelli et al., 1996; Victoria et al., 1991). This might explain the precipitation events with $d > +10$‰ observed in this study (Table 1). Therefore, the larger *d* during drought years

Table 2
Significant Relationships Between Event Precipitation Isotopes ($\delta^{18}O$, $\delta^{2}H$, $\delta^{17}O$, and d) and Local Meteorological Data From the National Botanic Research Institute, Windhoek, 2012–2016

Event precipitation isotope	Regression equation	r	R^2	p value
$\delta^{18}O$	$y = -0.24 \times$ (relative humidity) + 15.12	−0.63	0.39	**
	$y = 0.01 \times$ (lifted condensation level) − 8.79	0.61	0.37	**
	$y = -0.25 \times$ (precipitation amount) − 0.03	−0.42	0.18	**
	$y = 0.39 \times$ (surface temperature) − 13.47	0.29	0.08	**
	$y = 1.11 \times$ (wind speed) − 6.37	0.24	0.06	*
	$y = 0.56 \times$ (air temperature) − 13.27	0.24	0.06	*
$\delta^{2}H$	$y = -1.56 \times$ (relative humidity) + 98.22	−0.56	0.31	**
	$y = 0.06 \times$ (lifted condensation level) – 55.44	0.54	0.29	**
	$y = -1.69 \times$ (precipitation amount) + 1.23	−0.39	0.15	**
	$y = 8.62$ (wind speed) − 45.29	0.26	0.07	*
	$y = 2.47$ (surface temperature) − 83.02	0.25	0.06	*
$\delta^{17}O$	$y = -0.13$ (relative humidity) + 7.86	−0.62	0.39	**
	$y = 0.005$ (lifted condensation level) − 3.71	0.61	0.37	**
	$y = -0.13$ (precipitation amount) − 0.06	−0.42	0.18	**
	$y = 0.21$ (surface temperature) − 7.06	0.29	0.08	**
	$y = 0.58$ (wind speed) − 3.37	0.24	0.06	*
	$y = 0.29$ (air temperature) − 6.94	0.24	0.06	*
d	$y = -0.21$ (lifted condensation level) + 14.89	−0.68	0.47	**
	$y = 0.40$ (relative humidity) − 22.71	0.68	0.47	**
	$y = -1.78$ (air temperature) + 38.97	−0.50	0.28	**
	$y = 0.34$ (precipitation amount) + 1.49	0.40	0.16	**
	$y = -0.73$ (surface temperature) + 24.76	−0.37	0.14	**

*$p < 0.05$. **$p < 0.005$.

(+10.2‰) in the 300–600 m LCL bin suggests an increase in the evaporative flux due to moisture recycling, indicating drier conditions for the region compared to the normal year (+6.8‰), whose d was probably influenced more by subcloud evaporation.

3.3. Key Local Drivers of Precipitation Isotope Compositions

Precipitation isotopes are governed by several factors including but not limited to evaporation processes at the source, precipitation type, and subsequent rain-out processes along the air mass-trajectory; however, correlations with local meteorological parameters suggest possible modification at the precipitation site (Coplen et al., 2015; Dansgaard, 1964; Fudeyasu et al., 2011; Rindsberger et al., 1983; Salamalikis et al., 2016; Yurtsever, 1975). The Windhoek precipitation isotope data at both event and monthly scales exhibited significant relationships with local meteorological conditions (Tables 2 and S4, respectively). Whereas event-scale precipitation isotopes were related to more local meteorological parameters than monthly isotopes (six parameters versus three parameters), suggesting loss of information on individual events through data aggregation (Noone & Simmonds, 2002), these relationships were stronger at monthly scale (Risi et al., 2008; Vimeux et al., 2005; Wu et al., 2015). Therefore, event-scale comparisons with aggregated data will help define underlying uncertainties in relationships between isotopic composition of precipitation and climatic variables (Soderberg et al., 2013).

According to event-scale univariate analyses, the most significant local drivers of precipitation isotopes ($\delta^{18}O$, $\delta^{2}H$, and $\delta^{17}O$) in decreasing order were RH, LCL, precipitation amount, surface temperature, average wind speed, and air temperature (Table 2). Precipitation isotopes were inversely related to RH, which reflected the influence of subcloud evaporation on isotopic composition (Berkelhammer et al., 2012; Salamalikis et al., 2016; Table 2). This result was consistent with the Namibia precipitation isoscape that identified RH as a key driver of precipitation isotopes across Namibia (Kaseke et al., 2016). Precipitation isotopes were positively related to LCL, and this could be attributed to the raindrop travel time between the cloud base and ground surface, the longer this was the more time available for raindrop isotopic equilibration with subcloud vapor and subcloud evaporation (Salamalikis et al., 2016; Sánchez-Murillo et al., 2016; Table 2). Because LCL is a function of temperature and RH, RH and LCL are related (RH = −0.04 [LCL] + 99.00, $r = -0.999$, $R^2 = 0.998$,

Table 3
Best Performing Multiple Linear Regression Models Between Event Precipitation Isotopes and Local Meteorological Data From the National Botanic Research Institute, Windhoek, 2012–2016

Event Precipitation Isotope	Multiple linear regression equation	AIC	RSME	R^2	*p* value
$\delta^{18}O$	$y = 43.26 - (1.03 \times \text{air temp}) - (0.01 \times \text{amt}) - (0.34 \times \text{RH})$	300.9	4.5	0.53	<0.05
$\delta^{2}H$	$y = 334.28 - (8.62 \times \text{air temp}) - (0.70 \times \text{amt}) - (2.45 \times \text{RH})$	704.2	34.4	0.47	<0.05
$\delta^{17}O$	$y = 22.67 - (0.54 \times \text{air temp}) - (0.06 \times \text{amt}) - (0.18 \times \text{RH})$	174.0	2.4	0.53	<0.05
d	$y = 8.39 + (0.13 \times \text{amt}) - (0.02 \times \text{LCL}) + (1.68 \times \text{winspd})$	364.9	6.2	0.55	<0.05

Note. air temp = air temperature (°C); RH = relative humidity (%); amt = precipitation amount; LCL = lifted condensation level; winspd = wind speed (m/s). Only meteorological conditions with significant relationships from Table 2 were used.

$p < 0.005$), and this underlies the inverse relationship between *d* and LCL (Table 2). Precipitation isotopes were also inversely related to precipitation amount, and this could be attributed to the amount effect (Dansgaard, 1964). The amount effect suggests that light precipitation events are more prone to equilibration with enriched subcloud vapor and or experience subcloud evaporation and are thus more enriched than larger volume events. Larger precipitation events increase subcloud RH, reducing evaporation resulting in depleted isotope compositions compared to smaller events. This would result in positive relationships between *d* and precipitation amount and *d* and RH (Table 2). These results were thus consistent with expected subcloud evaporation from low intensity precipitation events over Windhoek. Finally, precipitation isotopes ($\delta^{18}O$, $\delta^{2}H$, and $\delta^{17}O$) showed weak but positive relationships with site air and surface temperature similar to Treble et al. (2005), which would enhance isotopic exchange with subcloud vapor as well as subcloud evaporation (Table 2). This was, however, in contrast to Dansgaard (1964) who did not observe a temperature effect using monthly data for the site.

At monthly timescales, the significant drivers of local precipitation isotope composition in decreasing order were RH, precipitation amount, and minimum temperature ($p < 0.05$; Table S4), while *d* was significantly related to a single local parameter RH (Table S4). Similar to the findings of Dansgaard (1964), volume-weighted monthly precipitation isotope compositions detected the amount effect indicating much stronger relationships than either the unweighted event or monthly samples but did not detect the *temperature effect* (Tables 2, S4, and S5). This suggests loss of information through data aggregation, temperature effect (Noone & Simmonds, 2002), while at the same time indicating that aridity is a major driver of precipitation isotope compositions at the site. Similarly, the weighted LMWL slope for this study 7.9 ± 0.35 ($n = 29$) was similar to that determined earlier 8 ± 1.5 ($n = 14$; Dansgaard, 1964), indicating subcloud evaporation and consistent with the interpretations above and classification of the site as semiarid (*BSh*).

Because multiscale influences on precipitation isotopes do not conform well to univariate regression analysis in midlatitude and subtropical locations (Alley & Cuffey, 2001; Fricke & O'Neil, 1999; Sturm et al., 2010), we applied multiple linear regression analysis (MLRA) at event scale (Table 3). The best performing models for $\delta^{18}O$, $\delta^{2}H$, and $\delta^{17}O$ combined air temperature, precipitation amount, and RH, accounting for 47–53% of isotope variability at the site (Table 3). However, the best performing model for *d* included precipitation amount, LCL, and average wind speed and accounted for 55% of the variation (Table 3). These MLRA models explained more precipitation isotope variation at event-scale compared to univariate analyses giving credence to the view that precipitation isotopes at midlatitude and subtropical locations do not lend well to univariate analysis (Tables 2 and 3). At the same time, these MLRA models suggest significant local modification of the precipitation isotope composition such that *d* cannot be considered a conservative environmental tracer of evaporation conditions at the source, at least for this semiarid site (Lai & Ehleringer, 2011; Welp et al., 2012; Zhao et al., 2014; Table 3). However, it is important to acknowledge that no analyses of source conditions was performed in this study. The most influential local parameter on precipitation isotope compositions over Windhoek according to the MLRA models was RH, suggesting isotopic exchange and subcloud evaporation associated with cloud base to ground surface travel time enhanced by air temperature as the physical mechanism accounting for 47–53% of $\delta^{18}O$, $\delta^{2}H$, and $\delta^{17}O$ variability. However, for *d*, LCL was the most influential parameter suggesting cloud base to ground surface travel time and associated subcloud evaporation with windy conditions as the driving physical mechanism (Tables 2 and 3).

The unaccounted precipitation isotope ($\delta^{18}O$, $\delta^{2}H$, and $\delta^{17}O$) variability from the MLRA models could be related to several factors including but not limited to precipitation type, rain-out processes, and source

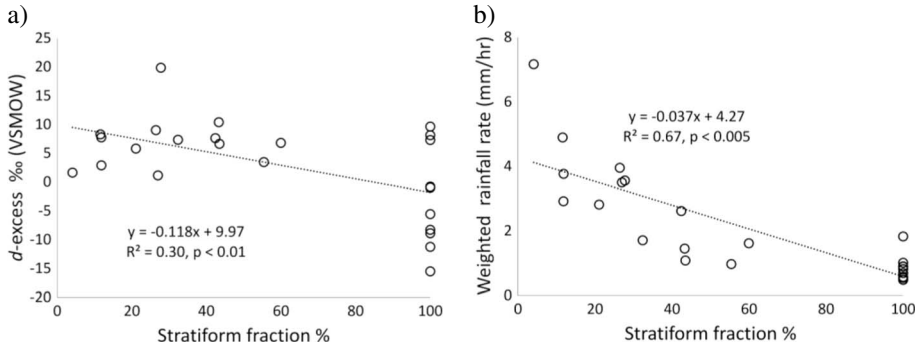

Figure 3. Variation of (a) *d*-excess as a function of stratiform fraction and (b) weighted conditional precipitation rate as a function of stratiform fraction, for rain events observed over Windhoek, 2012–2016 (n = 24). VSMOW = Vienna standard mean ocean water.

evaporation conditions (Aggarwal et al., 2016; Coplen et al., 2015; Crawford et al., 2013; Dansgaard, 1964; Fudeyasu et al., 2011; Jouzel et al., 2013). Recently, stratiform and convective precipitation have been associated with depleted and enriched isotopic compositions, respectively (Aggarwal et al., 2016; Coplen et al., 2015; Fudeyasu et al., 2011; Kurita, 2013). However, no significant relationships were observed between $\delta^{18}O$, $\delta^{2}H$, $\delta^{17}O$, and stratiform fraction at our study site, suggesting isotopic composition was independent of precipitation type (Table S6). This was supported by the significant inverse relationship between *d* and stratiform fraction (Figure 3a), suggesting stratiform precipitation was more susceptible to subcloud evaporation than convective precipitation. Stratiform precipitation consists of small raindrops (~1 mm in diameter) which may partially evaporate or grow by accretion and coalescence depending on prevailing conditions: subsidence or uplift, respectively (Houze Jr, 2014). Convective precipitation on the other hand consists of larger rain drops (>2 mm in diameter) that do not experience much evaporation or growth (Houze, 2014; Schumacher & Houze, 2003; Steiner & Smith, 1998). Therefore, an increase in stratiform fraction would diminish raindrop size, increase travel time from cloud base to ground surface, and decrease average precipitation rate facilitating subcloud evaporation and isotopic exchange with below cloud vapor. Models estimate a 30–80% reduction in raindrop size due to subcloud evaporation in arid environments, resulting from a combination of high temperatures and low RH (Wang et al., 2016). At the same time, the weighted precipitation rate decreased with an increase in stratiform fraction (Figure 3b), consistent with the predictions above enhancing equilibration with ambient vapor as well as enhancing subcloud evaporation. This would result in lower *d* and higher $\delta^{18}O$, $\delta^{2}H$, and $\delta^{17}O$ values for stratiform compared to convective precipitation which is less susceptible to subcloud evaporation (Houze, 2014; Schumacher & Houze Jr, 2003; Steiner & Smith, 1998), although this was only significant for *d* (Table S7).

Applying MLRA to *d*, the best performing model was $d = 4.0 - (0.12 \times \text{stratiform fraction}) + (0.56 \times \text{amount})$ (AIC = 82.9, $R^2 = 0.61$, RMSE = 5.3, $p < 0.05$), with precipitation amount being the most influential parameter. These results suggest that subcloud evaporation resulted in enrichment of ^{18}O, ^{2}H, and ^{17}O in stratiform precipitation to the extent that it was more enriched or similar to convective precipitation at the site (Table S7). This would explain the observed $\delta^{18}O$, $\delta^{2}H$, and $\delta^{17}O$ independence of precipitation type and rate observed at the site (Table S6). This contradicts the suggestion that the relationship between precipitation isotopes and intensity may be more visible at event scale (Dansgaard, 1964). This result could be related to the fact that precipitation type and intensity are related (Figure 3); thus, where both types occur, the influence of subcloud evaporation on the isotopic composition of the different precipitation types is not equal (Table S7). Therefore, the effect of precipitation intensity will likely be best observed when each precipitation type is considered separately or *d* is used instead (Table S6). However, given the data reduction already incurred in differentiating precipitation type, such an analysis is not possible for this study. These results therefore suggest that precipitation isotopes are independent of precipitation type at least at this site and possibly other dryland environments. However, it is important to acknowledge the complexity associated with these calculations; notably, estimation of stratiform fraction is greater when shallow rain is significant and amounts are low (Funk et al., 2013; Schumacher & Houze, 2003), while isotope data at a sampling point could be biased toward stratiform precipitation (point versus raster data; Aggarwal et al., 2016). Nonetheless, these calculations provide general trends of precipitation isotopes and precipitation type in a semiarid environment.

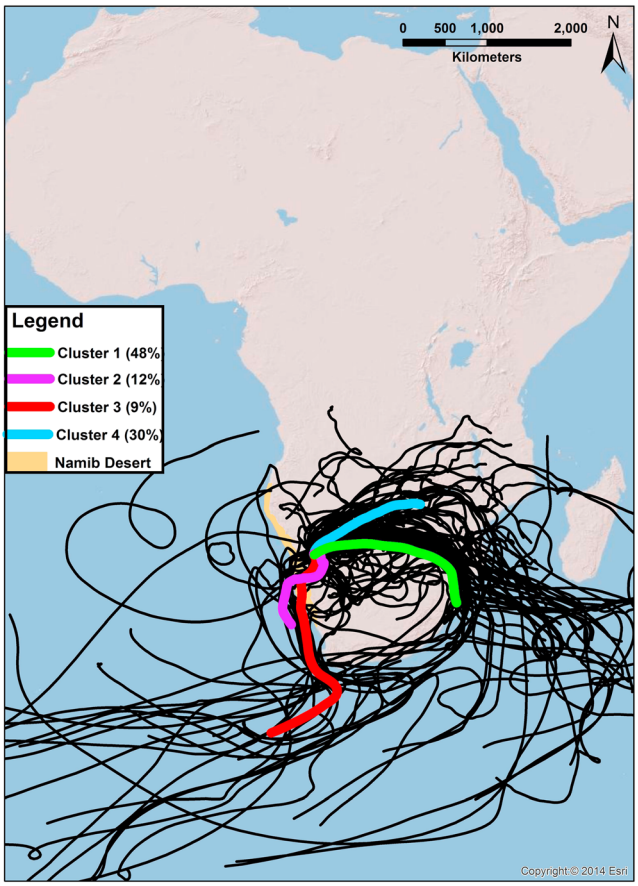

Figure 4. Ten-day (240 hr) atmospheric back trajectories of precipitation events received at Windhoek during the 2012–2016 period (n = 99). The associated mean trajectory clusters were based on ~6-day (140 hr) trajectories, which equate to the approximate travel time to Windhoek after intersecting land and atmospheric residence times for the region (Miralles et al., 2016).

3.4. HYSPLIT Air Mass Back Trajectories, Cluster Analysis, and $\delta'^{17}O$-$\delta'^{18}O$ Slopes

Ten-day HYSPLIT (Stein et al., 2015) back trajectory analyses suggest that Windhoek (2012–2016) precipitation originated from both the Indian and Atlantic Oceans (Figure 4). However, the 140-hr trajectory cluster analysis grouped the sources into four clusters (Figure 4), but no significant differences were detected among the precipitation clusters in $\delta^{18}O$, $\delta^{2}H$, $\delta^{17}O$, and d. This suggests that precipitation isotopes underwent extensive modification at the precipitation site (47–53%), making them indistinguishable (Table 3). The results highlight the inappropriateness of d as a conservative tracer of evaporation conditions at the source region, as 55% of d variability was related to local meteorological conditions at the precipitation site (Table 3). However, $^{17}\Delta$ and $\delta'^{17}O$-$\delta'^{18}O$ could be used as conservative tracers of humidity changes at the vapor source independent of temperature and thus complement d interpretations (Angert et al., 2004; Barkan & Luz, 2007; Li et al., 2015). The $\delta'^{17}O$-$\delta'^{18}O$ slopes of 0.529 ± 0.001 indicate a dominance of equilibrium fractionation processes, suggesting high RH conditions at the evaporation source (Luz & Barkan, 2005). Therefore, the $\delta'^{17}O$-$\delta'^{18}O$ slope of cluster 1 (0.529 ± 0.003) suggests high RH conditions over the subtropical Indian Ocean evaporation source (Figures 4 and 5). However, $\delta'^{17}O$-$\delta'^{18}O$ slopes of 0.506–0.5185 indicate a dominance of kinetic fractionation processes suggesting nonsteady state conditions with low RH at the evaporation source (Angert et al., 2004; Barkan & Luz, 2007). Thus, the $\delta'^{17}O$-$\delta'^{18}O$ slopes of clusters 2 (0.502 ± 0.007) and 3 (0.507 ± 0.019) suggest low RH conditions over the South Atlantic during evaporation (Figures 4 and 5). The $\delta'^{17}O$-$\delta'^{18}O$ slope for cluster 4 (0.520 ± 0.004) suggests nonsteady state evaporative conditions at more than 50% RH (Li et al., 2015). It is important to note that these trajectories only indicate geographic origins of moisture and do not take in account any additional moisture picked during transport to the site. We acknowledge that there seems to be an association between trajectory distance and $\delta'^{17}O$-$\delta'^{18}O$, suggesting an influence of ET on $\delta'^{17}O$-$\delta'^{18}O$ (Landais et al., 2006; Li et al., 2017; Figure 4). However, given that moisture recycling is estimated at 28–34% (Miralles et al., 2016), how and to what extent ET would influence precipitation $\delta'^{17}O$-$\delta'^{18}O$ in the region is uncertain (Landais et al., 2006; Li et al., 2017) and beyond the scope of the current study.

The origins of cluster 1 were consistent with the position of the subtropical Indian Ocean dipole (SIOD; Reason, 2001), while cluster 4 origins were consistent with the position of the tropical Indian Ocean dipole (Figure 4). SSTs around the origins of cluster 1 range from 23 to 26 °C, while those around cluster 4 origins range from 24 to 28 °C (October–April; Rao et al., 1989). Warmer SSTs would result in greater evaporation and result in higher RH over the tropical oceans (30°N–30°S; Shie et al., 2006). However, the $\delta'^{17}O$-$\delta'^{18}O$ slope of cluster 4 (0.520) was smaller than that of cluster 1 (0.529) despite higher SST around cluster 4 origins. This suggests nonsteady state conditions around cluster 4, resulting in lower RH than expected from the SST compared to cluster 1 origins. Summer precipitation in southern Africa has been associated with the tropical western Indian Ocean, with the subtropical southwest Indian Ocean thought to be a substantial source of moisture for the region (D'Abreton & Lindesay, 1993; Reason & Mulenga, 1999). However, the trajectory analyses results suggest that the subtropical Indian Ocean may contribute more moisture over the western parts of southern Africa or at least Windhoek (2012–2016) than the tropical Indian Ocean (Figure 4).

The third potential source of moisture associated with summer precipitation over southern Africa is often regarded as the tropical South Atlantic Ocean (Fauchereau et al., 2003; Hermes & Reason, 2005), although exact influences are unknown (Reason et al., 2006). However, our results suggest that clusters 2 and 3 originated from a region over the subtropical South Atlantic Ocean (Figure 4). It is known that West African precipitation is influenced by a South Atlantic Ocean dipole (SAOD), defined as northeast pole (10°E–20°W,

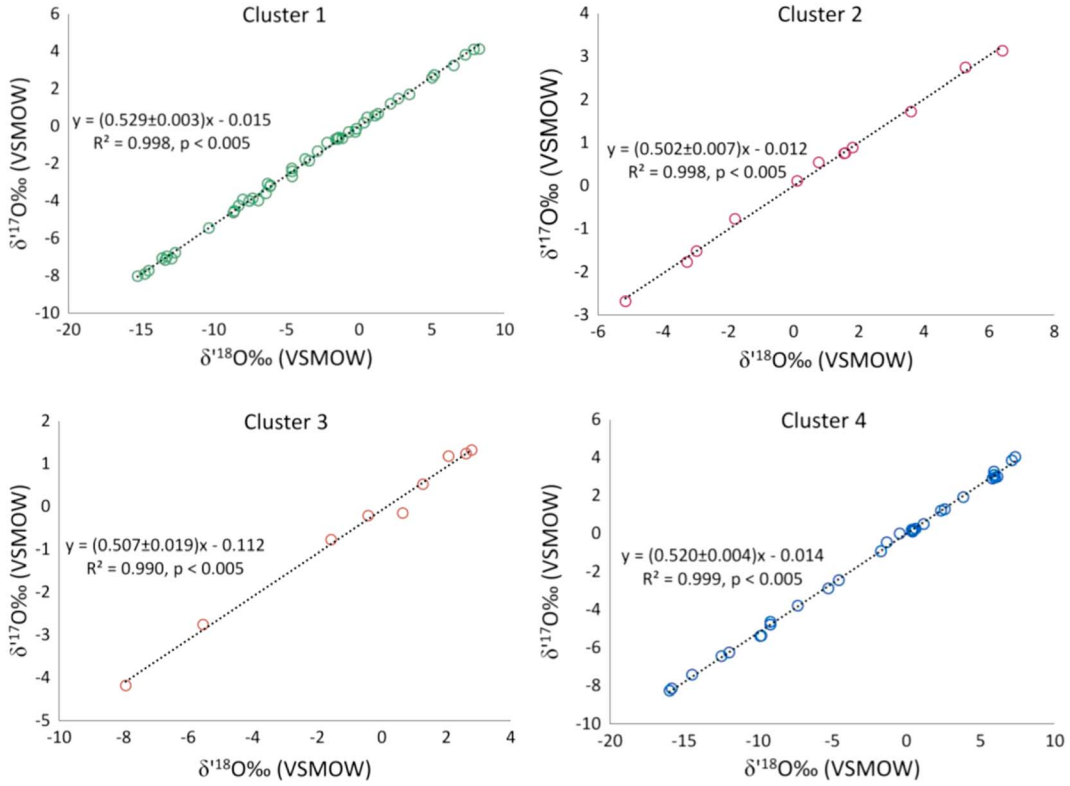

Figure 5. The four trajectory clusters of Windhoek precipitation during 2012–2016 as defined by the $\delta'^{17}O$-$\delta'^{18}O$ relationships. VSMOW = Vienna standard mean ocean water.

0–15°S) and southwest pole (10–40°W, 25–40°S; Nnamchi et al., 2011; Nnamchi & Li, 2011). However, simulations of this South Atlantic Ocean also suggest a smaller southeast pole (SEP) in phase with the northeast pole (Nnamchi et al., 2011), consistent with the origins of clusters 2 and 3, defined as SEP 0–15°E and 30–45°S (Figure S4). However, because Nnamchi and Li (2011) focused on SAOD influences on precipitation variability in West Africa, no attention was paid to possible influences on precipitation variability in southern Africa. Given that the results presented here and the simulations by Nnamchi et al. (2011) converge over the same region, they suggest that this SEP could be an extension of the SAOD or a secondary subtropical SAOD defined as SEP and southwest pole and may influence precipitation variability in southern Africa, at least over Windhoek (Figure S4). However, Reason and Jagadheesha (2005) and Harris et al. (2010) also suggest the existence of a subtropical SAOD influencing precipitation over the Southwestern Cape region of South Africa, although the location of the dipole is shifted slightly to the left of that proposed in Figure S4. Therefore, the existence of a subtropical SAOD is a distinct possibility, although exact locations may be debatable and outside the scope of this study. This is in contrast to studies that have often exclusively associated precipitation anomalies over western parts of central and southern Africa to the tropical South Atlantic Ocean, Benguela Niño and the SAOD (Hermes & Reason, 2005; Nnamchi & Li, 2011; Reason & Smart, 2015; Rouault, 2003).

Applying a simple classification based on oceanic origins of precipitation events over Windhoek (2012–2016), precipitation events were grouped into two: Indian Ocean (clusters 1 and 4) and subtropical Atlantic Ocean (clusters 2 and 3; Figures 4 and 6). The resulting $\delta'^{17}O$-$\delta'^{18}O$ slope for precipitation from the subtropical Atlantic Ocean (0.506 ± 0.009) was consistent with dominance of kinetic fractionation processes (0.506–0.5185), suggesting evaporation under nonsteady state conditions at low RH (Angert et al., 2004; Barkan & Luz, 2007; Li et al., 2015; Figure 6a). The $\delta'^{17}O$-$\delta'^{18}O$ slope for precipitation from the Indian Ocean (0.525 ± 0.002) was close to the 0.5265 slope which indicates evaporation occurred at high RH (~85%; Li et al., 2015; Figure 6b). According to Araguás-Araguás et al. (2000), high RH (~80%), warm temperatures (25 °C), and low wind velocities result in *d* values of about +10‰. Therefore, the $\delta'^{17}O$-$\delta'^{18}O$ results were consistent with

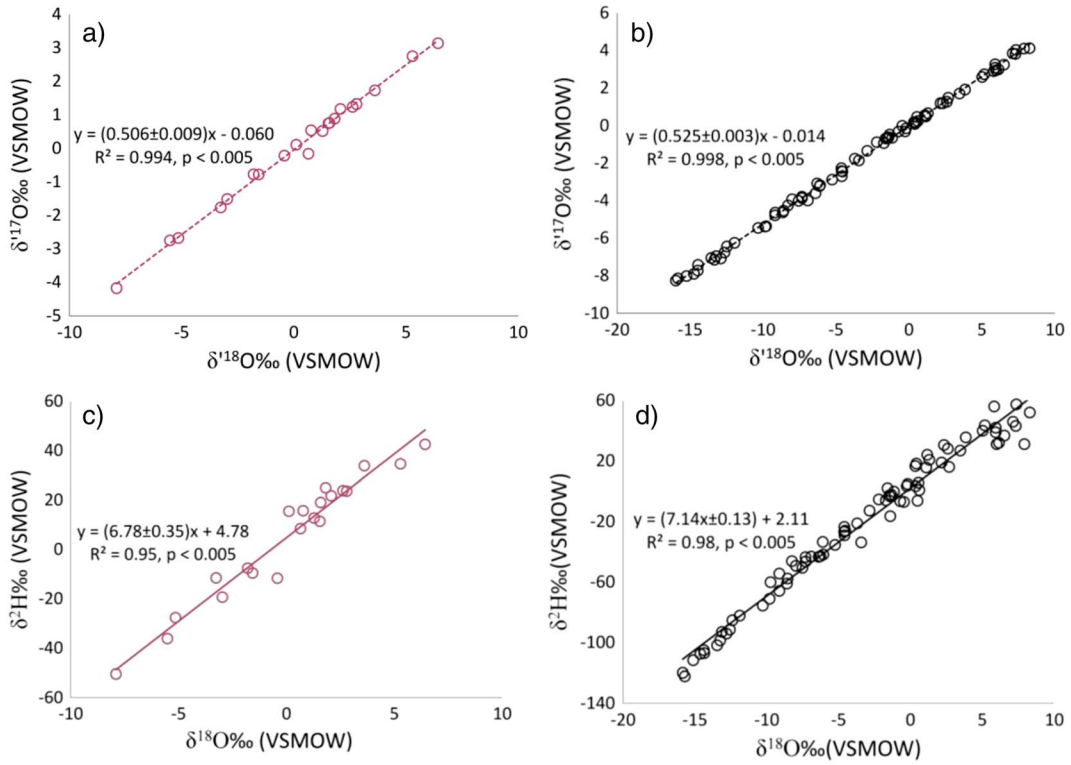

Figure 6. Isotope relationships of combined trajectory clusters based on ocean source for Windhoek precipitation 2012–2016; (a) subtropical Atlantic Ocean $\delta'^{17}O$-$\delta'^{18}O$, (b) Indian Ocean $\delta'^{17}O$-$\delta'^{18}O$, (c) subtropical Atlantic Ocean δ^2H-$\delta^{18}O$, and (d) Indian Ocean δ^2H-$\delta^{18}O$. VSMOW = Vienna standard mean ocean water.

SST and RH conditions for the Indian Ocean (Araguás-Araguás et al., 2000; Rao et al., 1989). However, precipitation *d* from the Indian (+7.7‰) and subtropical Atlantic Oceans (+5.5‰) were significantly smaller than the global meteoric water line (GMWL; +10‰; Kruskal-Wallis, $p < 0.05$; Mann-Whitney post hoc test, $p < 0.05$). There were no significant differences between precipitation *d* from the Indian and subtropical Atlantic Oceans (Kruskal-Wallis, $p > 0.05$) nor between their respective LMWLs (one-way ANCOVA, $p > 0.05$; Figures 6c and 6d). These results suggest that precipitation isotopes collected in Windhoek underwent significant modification by local meteorological conditions, consistent with earlier conclusions (Tables 2 and 3). These local modifications resulted in similar LMWLs (Figures 6c and 6d) and may have altered precipitation *d* by as much as 55% such that its use as a conservative tracer of evaporation conditions at the source may be questionable, at least for this semiarid environment (Table 3).

Precipitation from the subtropical Atlantic Ocean was significantly enriched in $\delta^{18}O$ (+0.8‰), δ^2H (+12.7‰), and $\delta^{17}O$ (+0.5‰) than from the Indian Ocean $\delta^{18}O$ (−2.0‰), δ^2H (−9.9‰), and $\delta^{17}O$ (−0.9‰; Kruskal-Wallis, $p < 0.05$). Because the Atlantic Ocean (~266 km) is located closer to Windhoek than the Indian Ocean (~1,904 km; Figures 1 and 4), the observed precipitation enrichment in $\delta^{18}O$, δ^2H, and $\delta^{17}O$ from events originating from the subtropical Atlantic Ocean could be reflecting the *continental effect* (Dansgaard, 1964). In addition, the isotope compositions of precipitation originating from the subtropical Atlantic Ocean presented here were generally more enriched in $\delta^{18}O$ and δ^2H compared to those reported for Cape Town (Harris et al., 2010). This could be attributed to the influence of subcloud evaporation at Windhoek as noted by Dansgaard (1964).

The Indian Ocean trajectories were the dominant source of Windhoek precipitation during 2012–2016, accounting for 68–92% of annual precipitation events and 51–94% of the annual precipitation amount (Table 4). These results were consistent with studies that have concluded that the Indian Ocean was the primary source of moisture for precipitation over southern Africa (D'Abreton & Lindesay, 1993; Reason & Mulenga, 1999; Reason & Smart, 2015). On the other hand, the results also indicate that the South Atlantic Ocean trajectories contributed a substantial amount of precipitation to Windhoek during this period,

Table 4
Annual and Total Contribution of Events and Precipitation From the Indian and South Atlantic Ocean over Windhoek 2012–2016

	2012–2013[a]		2013–2014[b]		2014–2015[a]		2015–2016[a]		2012–2016	
	Indian	Atlantic	Indian	Atlantic	Indian	Atlantic	Indian	Atlantic	Indian	Atlantic
% frq	71	29	92	8	76	24	68	32	79	21
% ppt	67	33	94	6	90	10	51	49	79	21

Note. frq = frequency; ppt = precipitation amount.
[a]drought year. [b]nondrought year.

24–32% of annual precipitation events and 10–49% of annual precipitation amount during drought years and 6–8% during nondrought years (Table 4). Therefore, more research is needed to understand the influence and effects of the subtropical South Atlantic Ocean on precipitation in Windhoek, Namibia, and southern Africa. It is important to acknowledge that the temporal isotopic variability for this subtropical semiarid site (Table 1) is similar to that of tropical sites, for example, Puerto Rico with different moisture sources (Sánchez-Murillo et al., 2016), suggesting some other pantropical mechanism may influence precipitation isotope compositions in addition to those described by Dansgaard (1964). Aggarwal et al. (2016) suggest that this mechanism could be the precipitation type, however, the results presented here contradicted this, suggesting that if such a pantropical mechanism exists, it requires further investigations.

3.5. Annual and Interannual LMWL

Figure 7 displays the different LMWLs generated for the site based on 2012–2016 event-scale data from the LMWL Freeware program (Crawford et al., 2014). Crawford et al. (2014) note that the calculation of LMWLs using different methods on the same data can result in wildly different LMWLs, complicating interpretation. However, for this particular site, LMWLs based on the unweighted methods were similar while those based on the weighted versions were similar, while both showed the same trends. The weighted LMWLs had larger slopes and intercepts than the unweighted LMWLs (Figure 7). However, these LMWLs were similar to those calculated for Windhoek based on GNIP data, $y = 7.1013x + 8.0159$ (OLSR) and $y = 7.30x + 9.3594$ (PWLSR; Crawford et al., 2014), except for the lower intercepts. The slope of the OLSR 2012–2016 LMWL (7.05) was significantly smaller than the GMWL (8; ANCOVA, $p < 0.05$), while GMWL *d* (+10‰) was significantly larger than that of the 2012–2016 Windhoek LMWL (+7.1‰; Kruskal-Wallis, $p < 0.05$; Figure 6). LMWLs with slopes <8 are characteristic of arid and semiarid environments (Araguás-Araguás et al., 2000), consistent with the classification of Windhoek as a hot semiarid climate (*BSh*). Arid and semiarid environments also suggest secondary processes such as subcloud evaporation (Ehhalt et al., 1963; Stewart, 1975), consistent with the low *d* observed at the site (Table 1).

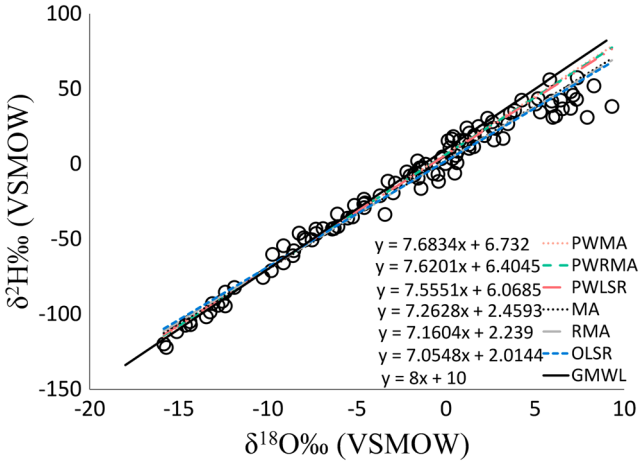

Figure 7. Event scale local meteoric water lines for Windhoek (2012–2016) calculated using Crawford et al. (2014) with the GMWL as a reference.
OLSR = ordinary least square regression; RMA = REDUCED major axis regression; MA = major axis regression; PW = precipitation weighted; VSMOW = Vienna standard mean ocean water; GMWL = global meteoric water line.

Whereas the 2012–2016 Windhoek LMWLs gave an overview of the general climate characteristics, they did not reflect annual variability, for example, wet versus dry years (Figure 8 and Table S1). There was no significant difference between the OLSR 2012–2016 LMWL (7.05) and 2013–2014 LMWL (7.36) slopes, suggesting *normal* precipitation amounts for the site during 2013–2014 (ANCOVA, $p > 0.05$; Figure 8b). However, the slopes of the OLSR LMWLs for 2012–2013 (6.57), 2014–2015 (6.42), and 2015–2016 (6.53) were significantly smaller than that of the 2012–2016 LMWL (7.05; ANCOVA, $p < 0.05$; Figure 8). The deviation of these annual LMWL slopes below the 2012–2016 LMWL reference suggest below normal precipitation during these periods at the site, consistent with the meteorological droughts observed (Figure 2 and Table S2). These results suggest that meteorological droughts caused abnormally dry conditions beyond the normal arid or semiarid conditions at the site. This would have resulted in enhanced or intense subcloud evaporation, significantly lowering annual LMWLs than the 2012–2016 LMWL (Figure 8). Therefore, the annual LMLs for

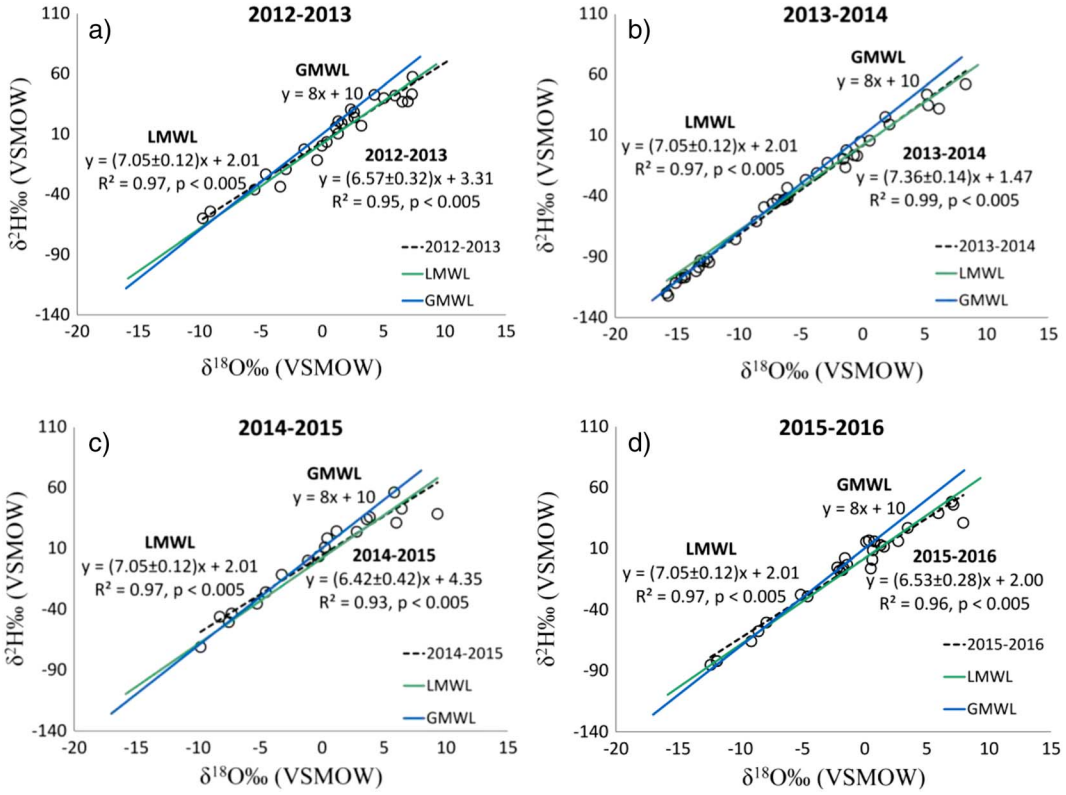

Figure 8. Annual unweighted LMWLs for Windhoek (2012–2016) based on the rainfall year (October–September): (a) 2012–2013, (b) 2013–2014, (c) 2014–2015, and (d) 2015–2016. The GMWL and unweighted LMWL (2012–2016) were included as references. LMWL = local meteoric water line; GMWL = global meteoric water line; VSMOW = Vienna standard mean ocean water.

2012–2013, 2014–2015, and 2015–2016 were consistent with the cumulative precipitation totals which indicated meteorological drought conditions during these years (Figure 2 and Table S2).

3.6. Drought Differentiation Using $\delta'^{17}O$-$\delta'^{18}O$ Relationship

There were no significant differences in precipitation *d* among the years 2012–2013 (+3.64‰), 2013–2014 (+7.33‰), 2014–2015 (+9.00‰), and 2015–2016 (+7.62‰) nor with the 2012–2016 LMWL (+7.13; Kruskal-Wallis, $p > 0.05$). This suggests that the precipitation isotopes were significantly altered by the local environmental parameters such that *d* was not a conservative tracer of evaporation conditions at the source. At the same time, there were no significant differences between LMWLs generated from precipitation events from the Indian Ocean ($y = 7.14 \pm 0.13x + 2.11 \pm 0.97$; $R^2 = 0.98$, $p < 0.05$) and those from the subtropical Atlantic Ocean ($y = 6.78 \pm 0.35x + 4.78 \pm 1.2$; $R^2 = 0.95$, $p < 0.05$; one-way ANCOVA, $p > 0.05$), suggesting that origins of precipitation had no effect on isotopic composition at the site. The $\delta'^{17}O$-$\delta'^{18}O$ slopes for 2012–2013 and 2013–2014 were similar (Figures 9a and 9b), suggesting high RH (~85%) evaporation conditions (Araguás-Araguás et al., 2000; Li et al., 2015) conducive for mass transport of moisture to the precipitation site (Figure 1). While Windhoek received normal to above normal precipitation during 2013–2014, consistent with expectations of an El Niño neutral year, 2012–2013 was a drought (Figures 2 and S1). However, the eastern and parts of central southern Africa (e.g., Mozambique, Zimbabwe, and Botswana) experienced above normal precipitation and violent storms during 2012–2013 (Moyo & Nangombe, 2015), while the western parts including Namibia experienced droughts. This suggests that Windhoek should have received normal to above normal precipitation during 2012–2013 but mesoscale (western southern Africa) conditions may have caused the drought. On the other hand, 2014–2015 and 2015–2016 $\delta'^{17}O$-$\delta'^{18}O$ slopes were similar (Figures 9c and 9d) and suggested low RH (~50%) nonsteady state evaporation conditions at the sources (Li et al., 2015), conditions that would have resulted in less moisture transported to the precipitation site (Figure 1). The 2014–2015 and 2015–2016 $\delta'^{17}O$-$\delta'^{18}O$ slopes thus possibly reflected El Niño (Figure S1), a

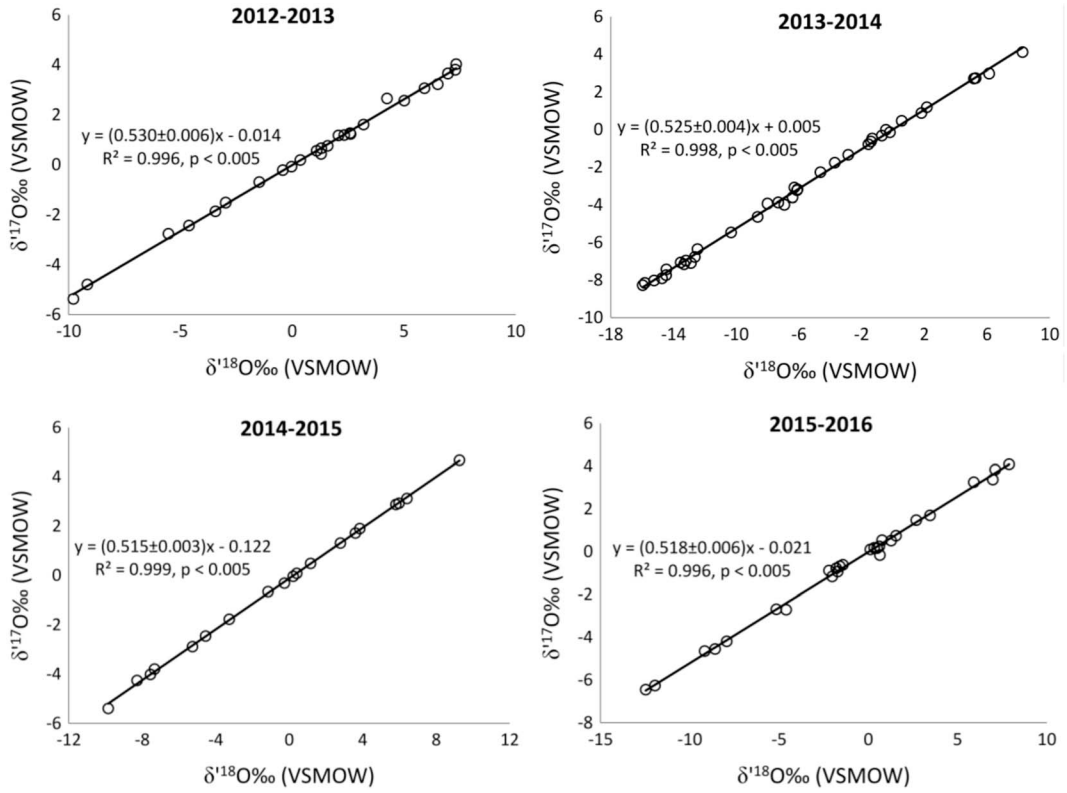

Figure 9. Plots showing the annual $\delta'^{17}O$-$\delta'^{18}O$ of Windhoek precipitation over 4 years. (a) 2012–2013, (b) 2013–2014, (c) 2014–2015, and (d) 2015–2016. VSMOW = Vienna standard mean ocean water.

synoptic system associated with droughts in the region (Hoell et al., 2016). Because 2012–2013 was ENSO neutral while the 2014–2016 droughts were probably El Niño related, $\delta'^{17}O$-$\delta'^{18}O$ could be reflecting differences in the causes of these droughts; mesoscale versus synoptic scale, respectively (Figure 9). These results were consistent with the increase (decrease) in recycled E/ET (T/ET) during 2014–2016 due to consecutive droughts that affected the entire region compared to the 2012–2013 drought which only affected the western parts of Southern Africa (Table S4). Interestingly, the origins of clusters 1 and 4 (Indian Ocean) were consistent with modeled source areas of precipitation deficits during droughts in the Kalahari ecoregion while clusters 2 and 3 (Atlantic Ocean) are not affected during droughts (Miralles et al., 2016; Figure 4). This decrease in Indian Ocean contributions to precipitation could account for the percentage increase in South Atlantic Ocean contributions during droughts observed at Windhoek (Table 4).

Because the correlation between $\delta^{18}O$ and $\delta^{2}H$ is controlled by underlying physical properties, it has been argued that PWRMA and PWMA are more appropriate approaches than OLSR, especially the former (Crawford et al., 2014). According to the PWRMA and PWMA LMWLs, the meteorological drought severity increased in the following order 2014–2015, 2015–2016, and 2012–2013 (Table S1). However, this was in contrast to the precipitation totals which suggest drought severity increased in the following order 2015–2016, 2014–2015, and 2012–2013 (Figure 2 and Table S2). Given the relationship between El Niño and droughts in the region (Allan et al., 2003; Nicholson & Entekhabi, 1986; Reason & Rouault, 2002), the 2015–2016 drought was expected to be more severe than the 2014–2015 based on El Niño strength (Figure S1). However, recent work suggests that precipitation response to drought in the region is related to ENSO and SIOD phase relationships (Hoell et al., 2016). A positive SIOD is characterized by warm waters on the southwest Indian Ocean and cool tropical waters in the central and eastern Indian Ocean, while a negative SIOD is reversed (Behera & Yamagata, 2001; Hoell et al., 2016; Reason, 2002). The warm waters of a positive SIOD increase evaporation, and the moist air is advected over southern Africa (Behera & Yamagata, 2001; Reason, 2001). When ENSO and SIOD are in phase (++), El Niño induced droughts are moderate, but when ENSO and SIOD are antiphase (+−), El Niño induced droughts are severe (Hoell et al., 2016). During early summer 2014–2015, El Niño and SIOD

Table 5
Multivariate Analysis of Windhoek Precipitation as Influenced by El Niño–Southern Oscillation and the SWIO Index nodes (2012–2016)

	Multiple linear regression equation	AIC	RSME	R^2	*p* value
ppt (mm)	$y = 27.61 - (15.32 \times \text{MEI}) + (37.07 \times \text{SWIO})$	337.3	32.6	0.17	<0.05

Note. ppt = monthly precipitation amount; SWIO = South Western Indian Ocean; MEI = multivariate ENSO index; ENSO = El Niño–Southern Oscillation.

were antiphase (Figures S1 and S3), and this may have enhanced the precipitation response to El Niño, less precipitation than expected (Figure 2 and Table S2). On the other hand, 2015–2016 experienced a stronger ENSO (+) but was in phase with the SIOD (+; Figures S1 and S3), mitigating the precipitation response to El Niño, more precipitation than expected (Figure 2 and Table S2).

Neither univariate analyses nor MLRA showed any significant relationships between precipitation amount, ONI, and the SIOD as measured by the South Western Indian Ocean index (http://stateoftheocean.osmc.noaa.gov/sur/ind/swio.php; Ocean Observations Panel for Climate, 2016; $p > 0.05$). This could be because ENSO is a result of complex interactions between several climate systems, thus the multivariate ENSO index (MEI; https://www.esrl.noaa.gov/psd/enso/mei/table.html; NOAA, 2016) was substituted for ONI. MEI is considered the most representative ENSO index integrating multiple meteorological parameters measured over the Pacific Ocean (Mazzarella et al., 2013). Multiple linear regression analyses showed a significant relationship ($p < 0.05$) between precipitation amount, MEI, and South Western Indian Ocean accounting for 17.4% of precipitation variability observed in Windhoek (2012–2016; Table 5). These results suggest that precipitation amount over the site may have been partly related to the interaction of the SIOD and ENSO nodes, consistent with Hoell et al. (2016; Figures 2, S1, and S3). We did not perform a similar analysis for the South Atlantic Ocean because the northeastern pole of the current SAOD indices are based on the northeastern parts of the South Atlantic (http://stateoftheocean.osmc.noaa.gov/sur/atl/sat.php; Nnamchi et al., 2011; Ocean Observations Panel for Climate, 2017) versus the southeastern parts identified in this study (Figure S4). Therefore, the current SAOD Index does not represent the region of interest and is thus inappropriate for this study (Figure S4). Furthermore, there is little research related to the influence of the subtropical Atlantic on precipitation across southern Africa.

4. Conclusions

Precipitation isotopes sampled from Windhoek over the period 2012–2016 suggest significant modification by local meteorological parameters, accounting for 47–53% of the isotope variability. The most influential local meteorological parameters at both event and monthly scales indicated substantial subcloud evaporation at the site, consistent with the semiarid classification of the site and the meteorological droughts that occurred during this period. At the same time, subcloud evaporation may have resulted in significant modification of stratiform precipitation such that it was indistinguishable from convective precipitation using individual isotopes, resulting in isotopic compositions ($\delta^{18}O$, $\delta^{2}H$, and $\delta^{17}O$) that were independent of precipitation type. This suggests that precipitation $\delta^{18}O$, $\delta^{2}H$, and $\delta^{17}O$ in arid and semiarid environments could be independent of precipitation type, at least for Windhoek. However, it is still possible to differentiate stratiform precipitation from convection precipitation based on *d*. Trajectory analyses suggested that precipitation events experienced at the site could be broadly classified into two groups: Indian and subtropical South Atlantic Ocean sourced. Contrary to popular perception, these results suggest that the subtropical South Atlantic Ocean generates a nonnegligible amount of precipitation events over Windhoek. Therefore, the influence of the subtropical South Atlantic Ocean on southern African precipitation and climate could currently be underestimated. At the same time, $\delta'^{17}O$-$\delta'^{18}O$ in conjunction with HYSPLIT back trajectories identified four precipitation source clusters. Two of these cluster sources were consistent with the positions of the Indian Ocean dipole and the SOID, while the remaining clusters had similar origins in the subtropical South Atlantic Ocean, consistent with simulations of a possible dipole in the subtropical South Atlantic Ocean (Nnamchi et al., 2011). If such a dipole exists, this could influence precipitation over southern Africa, and understanding it would improve forecasting efforts over the region or at least Windhoek and parts of South Africa. $\delta'^{17}O$-$\delta'^{18}O$ appeared a much better tracer of environmental conditions at the evaporation site than *d* which was significantly influenced by meteorological conditions at the precipitation site. At the same time, $\delta'^{17}O$-$\delta'^{18}O$ appeared to reflect differences between El Niño and non-El Niño related droughts, suggesting $\delta'^{17}O$-$\delta'^{18}O$ could be a novel tool to differentiate drought causes; synoptic versus mesoscale, respectively. Finally, the temporal isotope variability exhibited by this semiarid site compared to some tropical sites suggests that some pantropical mechanism may be controlling precipitation isotope compositions but the nature of this mechanism we believe is still elusive.

Acknowledgments

Funding for this work was made available from the U.S. National Science Foundation (IIA-1427642 and EAR-1554894). The data used are listed in the references, tables, and in Table S1. We thank three anonymous reviewers for their insightful comments and constructive suggestions to improve the quality of this manuscript.

References

Aggarwal, P. K., Romatschke, U., Araguas-Araguas, L., Belachew, D., Longstaffe, F. J., Berg, P., et al. (2016). Proportions of convective and stratiform precipitation revealed in water isotope ratios. *Nature Geoscience*, *9*(8), 624–629. https://doi.org/10.1038/ngeo2739

Allan, R., Reason, C., Lindesay, J., & Ansell, T. (2003). Protracted ENSO episodes and their impacts in the Indian Ocean region. *Deep Sea Research Part II: Topical Studies in Oceanography*, *50*(12-13), 2331–2347. https://doi.org/10.1016/S0967-0645(03)00059-6

Alley, R. B., & Cuffey, K. M. (2001). Oxygen- and hydrogen-isotopic ratios of water in precipitation: Beyond paleothermometry. *Reviews in Mineralogy and Geochemistry*, *43*(1), 527–553. https://doi.org/10.2138/gsrmg.43.1.527

Angert, A., Cappa, C. D., & DePaolo, D. J. (2004). Kinetic ^{17}O effects in the hydrologic cycle: Indirect evidence and implications. *Geochimica et Cosmochimica Acta*, *68*(17), 3487–3495. https://doi.org/10.1016/j.gca.2004.02.010

Araguás-Araguás, L., Froehlich, K., & Rozanski, K. (2000). Deuterium and $\delta^{18}O$ isotope composition of precipitation and atmospheric moisture. *Hydrological Processes*, *14*(8), 1341–1355. https://doi.org/10.1002/1099-1085(20000615)14:8<1341::AID-HYP983>3.0.CO;2-Z

Baldini, L. M., McDermott, F., Baldini, J. U., Fischer, M. J., & Möllhoff, M. (2010). An investigation of the controls on Irish precipitation δ18O values on monthly and event timescales. *Climate Dynamics*, *35*(6), 977–993. https://doi.org/10.1007/s00382-010-0774-6

Barkan, E., & Luz, B. (2007). Diffusivity fractionations of $H_2{}^{16}O/H_2{}^{17}O$ and $H_2{}^{16}O/H_2{}^{18}O$ in air and their implications for isotope hydrology. *Rapid Communications in Mass Spectrometry*, *21*(18), 2999–3005. https://doi.org/10.1002/rcm.3180

Barras, V., & Simmonds, I. (2009). Observation and modeling of stable water isotopes as diagnostics of rainfall dynamics over southeastern Australia. *Journal of Geophysical Research*, *114*, D23308. https://doi.org/10.1029/2009JD012132

Barras, V. J., & Simmonds, I. (2008). Synoptic controls upon δ18O in southern Tasmanian precipitation. *Geophysical Research Letters*, *35*, L02707. https://doi.org/10.1029/2007GL031835

Behera, S. K., & Yamagata, T. (2001). Subtropical SST dipole events in the southern Indian Ocean. *Geophysical Research Letters*, *28*, 327–330. https://doi.org/10.1029/2000GL011451

Benson, L., & Klieforth, H. (1989). Stable isotopes in precipitation and ground water in the Yucca Mountain region, southern Nevada: Paleoclimatic implications. In *Aspects of climate variability in the Pacific and the western Americas* (pp. 41–59). Washington, DC: American Geophysical Union.

Berkelhammer, M., Stott, L., Yoshimura, K., Johnson, K., & Sinha, A. (2012). Synoptic and mesoscale controls on the isotopic composition of precipitation in the western United States. *Climate Dynamics*, *38*(3–4), 433–454. https://doi.org/10.1007/s00382-011-1262-3

Bowen, G., & Revenaugh, J. (2003). Interpolating the isotopic composition of modern meteoric precipitation. *Water Resources Research*, *39*(10), 1299. https://doi.org/10.1129/2003WR002086

Bowen, G. J. (2017). The Online Isotopes in Precipitation Calculator. Retrieved from http://www.waterisotopes.org

Burnett, A. W., Mullins, H. T., & Patterson, W. P. (2004). Relationship between atmospheric circulation and winter precipitation δ18O in central New York State. *Geophysical Research Letters*, *31*, L22209. https://doi.org/10.1029/2004GL021089

Conway, D., Van Garderen, E. A., Deryng, D., Dorling, S., Krueger, T., Landman, W., et al. (2015). Climate and southern Africa's water-energy-food nexus. *Nature Climate Change*, *5*(9), 837–846. https://doi.org/10.1038/nclimate2735

Coplen, T. B., Neiman, P. J., White, A. B., & Ralph, F. M. (2015). Categorisation of northern California rainfall for periods with and without a radar brightband using stable isotopes and a novel automated precipitation collector. *Tellus Series B: Chemical and Physical Meteorology*, *67*(1), 28574. https://doi.org/10.3402/tellusb.v67.28574

Climate Prediction Center (2016). Oceanic Nino Index (ONI), in *Cold and Warm Seasons*, Edited, Climate Prediction Center.

Crawford, J., Hughes, C. E., & Lykoudis, S. (2014). Alternative least squares methods for determining the meteoric water line, demonstrated using GNIP data. *Journal of Hydrology*, *519*, 2331–2340. https://doi.org/10.1016/j.jhydrol.2014.10.033

Crawford, J., Hughes, C. E., & Parkes, S. D. (2013). Is the isotopic composition of event based precipitation driven by moisture source or synoptic scale weather in the Sydney Basin, Australia? *Journal of Hydrology*, *507*, 213–226. https://doi.org/10.1016/j.jhydrol.2013.10.031

D'Abreton, P., & Lindesay, J. (1993). Water vapour transport over southern Africa during wet and dry early and late summer months. *International Journal of Climatology*, *13*(2), 151–170. https://doi.org/10.1002/joc.3370130203

Dansgaard, W. (1964). Stable isotopes in precipitation. *Tellus*, *16*, 436–468.

Ehhalt, D., Knott, K., Nagel, J., & Vogel, J. (1963). Deuterium and $\delta^{18}O$ in rain water. *Journal of Geophysical Research*, *68*(13), 3775–3780. https://doi.org/10.1029/JZ068i013p03775

Fauchereau, N., Trzaska, S., Richard, Y., Roucou, P., & Camberlin, P. (2003). Sea-surface temperature co-variability in the Southern Atlantic and Indian Oceans and its connections with the atmospheric circulation in the Southern Hemisphere. *International Journal of Climatology*, *23*(6), 663–677. https://doi.org/10.1002/joc.905

Field, R. D. (2010). Observed and modeled controls on precipitation δ18O over Europe: From local temperature to the Northern Annular Mode. *Journal of Geophysical Research*, *115*, D12101. https://doi.org/10.1029/2009JD013370

Fricke, H. C., & O'Neil, J. R. (1999). The correlation between 18 O/16 O ratios of meteoric water and surface temperature: Its use in investigating terrestrial climate change over geologic time. *Earth and Planetary Science Letters*, *170*(3), 181–196. https://doi.org/10.1016/S0012-821X(99)00105-3

Friedman, I., Harris, J. M., Smith, G. I., & Johnson, C. A. (2002). Stable isotope composition of waters in the Great Basin, United States 1. Air-mass trajectories. *Journal of Geophysical Research*, *107*(D19), 4401. https://doi.org/10.1029/2001JD000565

Fudeyasu, H., Ichiyanagi, K., Yoshimura, K., Mori, S., Hamada, J.-I., Sakurai, N., et al. (2011). Effects of large-scale moisture transport and mesoscale processes on precipitation isotope ratios observed at Sumatera, Indonesia. *Journal of the Meteorological Society of Japan. Ser. II*, *89*, 49–59.

Funk, A., Schumacher, C., & Awaka, J. (2013). Analysis of rain classifications over the tropics by version 7 of the TRMM PR 2A23 algorithm. *Journal of the Meteorological Society of Japan. Ser. II*, *91*(3), 257–272. https://doi.org/10.2151/jmsj.2013-302

Gat, J. (1996). Oxygen and hydrogen isotopes in the hydrologic cycle. *Annual Review of Earth and Planetary Sciences*, *24*(1), 225–262. https://doi.org/10.1146/annurev.earth.24.1.225

Gat, J., & Matsui, E. (1991). Atmospheric water balance in the Amazon Basin: An isotopic evapotranspiration model. *Journal of Geophysical Research*, *96*(D7), 13,179–13,188. https://doi.org/10.1029/91JD00054

Gat, J. R., & Carmi, I. (1970). Evolution of the isotopic composition of atmospheric waters in the Mediterranean Sea area. *Journal of Geophysical Research*, *75*, 3039–3048. https://doi.org/10.1029/JC075i015p03039

Hammer, Ø., Harper, D. A. T., & Ryan, P. D. (2001). PAST: Paleontological statistics software package for education and data analysis. *Palaeontologia Electronica*, *4*(1), 9.

Harris, C., Burgers, C., Miller, J., & Rawoot, F. (2010). O- and H-isotope record of Cape Town rainfall from 1996 to 2008, and its application to recharge studies of Table Mountain groundwater, South Africa. *South African Journal of Geology*, *113*(1), 33–56. https://doi.org/10.2113/gssajg.113.1.33

Hermes, J., & Reason, C. (2005). Ocean model diagnosis of interannual coevolving SST variability in the South Indian and South Atlantic Oceans. *Journal of Climate*, *18*(15), 2864–2882. https://doi.org/10.1175/JCLI3422.1

Hoell, A., Funk, C., Zinke, J., & Harrison, L. (2016). Modulation of the Southern Africa precipitation response to the El Niño Southern Oscillation by the subtropical Indian Ocean Dipole. *Climate Dynamics*, *48*(7-8), 2529–2540. https://doi.org/10.1007/s00382-016-3220-6

Houze, R. A. Jr. (2014). *Cloud dynamics* (2nd ed., p. 432). Oxford: Elsevier Academic Press.

Hulston, J., & Thode, H. (1965). Variations in the S^{33}, S^{34}, and S^{36} contents of meteorites and their relation to chemical and nuclear effects. *Journal of Geophysical Research*, *70*(14), 3475–3484. https://doi.org/10.1029/JZ070i014p03475

Jouzel, J., Delaygue, G., Landais, A., Masson-Delmotte, V., Risi, C., & Vimeux, F. (2013). Water isotopes as tools to document oceanic sources of precipitation. *Water Resources Research*, *49*, 7469–7486. https://doi.org/10.1002/2013WR013508

Kaseke, K. F., Wang, L., & Seely, M. K. (2017). Nonrainfall water origins and formation mechanisms. *Science Advances*, *3*(3), e1603131. https://doi.org/10.1126/sciadv.1603131

Kaseke, K. F., Wang, L., Wanke, H., Turewicz, V., & Koeniger, P. (2016). An analysis of precipitation isotope distributions across Namibia using historical data. *PLoS One*, *11*(5), e0154598. https://doi.org/10.1371/journal.pone.0154598

Kazmierz Rozanski, L. A.-A., & Gonftanttni, R. (1993). Isotopic patterns in modern global precipitation.

Kurita, N. (2013). Water isotopic variability in response to mesoscale convective system over the tropical ocean. *Journal of Geophysical Research*, *118*, 10,376–10,390. https://doi.org/10.1002/jgrd.50754

Läderach, A., & Sodemann, H. (2016). A revised picture of the atmospheric moisture residence time. *Geophysical Research Letters*, *43*, 924–933. https://doi.org/10.1002/2015GL067449

Lai, C. T., & Ehleringer, J. R. (2011). Deuterium excess reveals diurnal sources of water vapor in forest air. *Oecologia*, *165*(1), 213–223. https://doi.org/10.1007/s00442-010-1721-2

Landais, A., Barkan, E., Yakir, D., & Luz, B. (2006). The triple isotopic composition of oxygen in leaf water. *Geochimica et Cosmochimica Acta*, *70*(16), 4105–4115. https://doi.org/10.1016/j.gca.2006.06.1545

Lawrence, M. G. (2005). The relationship between relative humidity and the dewpoint temperature in moist air: A simple conversion and applications. *Bulletin of the American Meteorological Society*, *86*(2), 225–234. https://doi.org/10.1175/BAMS-86-2-225

Lee, J. E., Fung, I., DePaolo, D. J., & Henning, C. C. (2007). Analysis of the global distribution of water isotopes using the NCAR atmospheric general circulation model. *Journal of Geophysical Research*, *112*, D16306. https://doi.org/10.1029/2006JD007657

Lewis, S., LeGrande, A., Kelley, M., & Schmidt, G. (2010). Water vapour source impacts on oxygen isotope variability in tropical precipitation during Heinrich events. *Climate of the Past*, *6*(3), 325–343. https://doi.org/10.5194/cp-6-325-2010

Li, S., Levin, N. E., & Chesson, L. A. (2015). Continental scale variation in 17 O-excess of meteoric waters in the United States. *Geochimica et Cosmochimica Acta*, *164*, 110–126. https://doi.org/10.1016/j.gca.2015.04.047

Li, S., Levin, N. E., Soderberg, K., Dennis, K. J., & Caylor, K. K. (2017). Triple oxygen isotope composition of leaf waters in Mpala, central Kenya. *Earth and Planetary Science Letters*, *468*, 38–50. https://doi.org/10.1016/j.epsl.2017.02.015

Liu, J., Fu, G., Song, X., Charles, S. P., Zhang, Y., Han, D., & Wang, S. (2010). Stable isotopic compositions in Australian precipitation. *Journal of Geophysical Research*, *115*, D23307. https://doi.org/10.1029/2010JD014403

Liu, J., Song, X., Fu, G., Liu, X., Zhang, Y., & Han, D. (2011). Precipitation isotope characteristics and climatic controls at a continental and an island site in Northeast Asia. *Climate Research*, *49*(1), 29–44. https://doi.org/10.3354/cr01013

Lu, X., Wang, L., Pan, M., Kaseke, K. F., & Li, B. (2016). A multi-scale analysis of Namibian rainfall over the recent decade–comparing TMPA satellite estimates and ground observations. *Journal of Hydrology: Regional Studies*, *8*, 59–68.

Luz, B., & Barkan, E. (2005). The isotopic ratios $^{17}O/^{16}O$ and $^{18}O/^{16}O$ in molecular oxygen and their significance in biogeochemistry. *Geochimica et Cosmochimica Acta*, *69*(5), 1099–1110. https://doi.org/10.1016/j.gca.2004.09.001

Martinelli, L. A., Victoria, R. L., Sternberg, L. S. L., Ribeiro, A., & Moreira, M. Z. (1996). Using stable isotopes to determine sources of evaporated water to the atmosphere in the Amazon basin. *Journal of Hydrology*, *183*(3-4), 191–204. https://doi.org/10.1016/0022-1694(95)02974-5

Mazzarella, A., Giuliacci, A., & Scafetta, N. (2013). Quantifying the Multivariate ENSO Index (MEI) coupling to CO_2 concentration and to the length of day variations. *Theoretical and Applied Climatology*, *111*(3–4), 601–607. https://doi.org/10.1007/s00704-012-0696-9

Merlivat, L., & Jouzel, J. (1979). Global climatic interpretation of the deuterium-18O relationship for precipitation. *Journal of Geophysical Research*, *84*(C8), 5029–5033. https://doi.org/10.1029/JC084iC08p05029

Miller, M. F. (2002). Isotopic fractionation and the quantification of ^{17}O anomalies in the oxygen three-isotope system: An appraisal and geochemical significance. *Geochimica et Cosmochimica Acta*, *66*(11), 1881–1889. https://doi.org/10.1016/S0016-7037(02)00832-3

Miralles, D. G., Nieto, R., McDowell, N. G., Dorigo, W. A., Verhoest, N. E., Liu, Y. Y., et al. (2016). Contribution of water-limited ecoregions to their own supply of rainfall. *Environmental Research Letters*, *11*(12), 124007. https://doi.org/10.1088/1748-9326/11/12/124007

Moyo, E. N., & Nangombe, S. S. (2015). Southern Africa's 2012–13 violent storms: Role of climate change. *Procedia IUTAM*, *17*, 69–78. https://doi.org/10.1016/j.piutam.2015.06.011

Munday, C., & Washington, R. (2017). Circulation controls on southern African precipitation in coupled models: The role of the Angola low. *Journal of Geophysical Research: Atmospheres*, *122*, 861–877. https://doi.org/10.1002/2016JD025736

Nicholson, S. E., & Entekhabi, D. (1986). The quasi-periodic behavior of rainfall variability in Africa and its relationship to the Southern Oscillation. *Meteorology and Atmospheric Physics*, *34*(3), 311–348.

Nnamchi, H. C., & Li, J. (2011). Influence of the South Atlantic Ocean dipole on West African summer precipitation. *Journal of Climate*, *24*(4), 1184–1197. https://doi.org/10.1175/2010JCLI3668.1

Nnamchi, H. C., Li, J., & Anyadike, R. N. (2011). Does a dipole mode really exist in the South Atlantic Ocean? *Journal of Geophysical Research*, *116*, D15104. https://doi.org/10.1029/2010JD015579

NOAA (2016). Multivariate El Niño Southern Oscillation (MEI) index edited by K. Wolter, National Oceanic and Atmospheric Administration (NOAA).

Noone, D., & Simmonds, I. (2002). Associations between δ 18O of water and climate parameters in a simulation of atmospheric circulation for 1979–95. *Journal of Climate*, *15*(22), 3150–3169. https://doi.org/10.1175/1520-0442(2002)015<3150:ABOOWA>2.0.CO;2

Ocean Observations Panel for Climate (2016). South Western Indian Ocean (SWIO) SST, Edited by OOPC, Ocean Observations Panel for Climate

Ocean Observations Panel for Climate (2017). South Atlantica Tropical (SAT) SST index, edited, Ocean Observations Panel for Climate.

Rao, R. R., Molinari, R. L., & Festa, J. F. (1989). Evolution of the climatological near-surface thermal structure of the tropical Indian Ocean: 1. Description of mean monthly mixed layer depth, and sea surface temperature, surface current, and surface meteorological fields. *Journal of Geophysical Research*, *94*(C8), 10,801–10,815. https://doi.org/10.1029/JC094iC08p10801

Reason, C. (2001). Subtropical Indian Ocean SST dipole events and southern African rainfall. *Geophysical Research Letters*, *28*(11), 2225–2227. https://doi.org/10.1029/2000GL012735

Reason, C. (2002). Sensitivity of the southern African circulation to dipole sea-surface temperature patterns in the South Indian Ocean. *International Journal of Climatology*, *22*(4), 377–393. https://doi.org/10.1002/joc.744

Reason, C., & Jagadheesha, D. (2005). Relationships between South Atlantic SST variability and atmospheric circulation over the South African region during austral winter. *Journal of Climate*, *18*(16), 3339–3355. https://doi.org/10.1175/JCLI3474.1

Reason, C., Landman, W., & Tennant, W. (2006). Seasonal to decadal prediction of southern African climate and its links with variability of the Atlantic Ocean. *Bulletin of the American Meteorological Society*, *87*(7), 941–956. https://doi.org/10.1175/BAMS-87-7-941

Reason, C., & Mulenga, H. (1999). Relationships between South African rainfall and SST anomalies in the Southwest Indian Ocean. *International Journal of Climatology*, *19*(15), 1651–1673. https://doi.org/10.1002/(SICI)1097-0088(199912)19:15<1651::AID-JOC439>3.0.CO;2-U

Reason, C., & Rouault, M. (2002). ENSO-like decadal variability and South African rainfall. *Geophysical Research Letters*, *29*(13), 1638. https://doi.org/10.1029/2002GL014663

Reason, C. J., & Smart, S. (2015). Tropical south east Atlantic warm events and associated rainfall anomalies over southern Africa. *Frontiers in Environmental Science*, *3*, 24.

Richard, Y., Trzaska, S., Roucou, P., & Rouault, M. (2000). Modification of the southern African rainfall variability/ENSO relationship since the late 1960s. *Climate Dynamics*, *16*(12), 883–895. https://doi.org/10.1007/s003820000086

Rindsberger, M., Magaritz, M., Carmi, I., & Gilad, D. (1983). The relation between air mass trajectories and the water isotope composition of rain in the Mediterranean Sea area. *Geophysical Research Letters*, *10*, 43–46. https://doi.org/10.1029/GL010i001p00043

Risi, C., Bony, S., & Vimeux, F. (2008). Influence of convective processes on the isotopic composition (δ18O and δD) of precipitation and water vapor in the tropics: 2. Physical interpretation of the amount effect. *Journal of Geophysical Research*, *113*, D19305. https://doi.org/10.1029/2008JD009942

Risi, C., Bony, S., Vimeux, F., & Jouzel, J. (2010). Water-stable isotopes in the LMDZ4 general circulation model: Model evaluation for present-day and past climates and applications to climatic interpretations of tropical isotopic records. *Journal of Geophysical Research*, *115*, D12118. https://doi.org/10.1029/2009JD013255

Romps, D. M. (2017). Exact expression for the lifting condensation level. *Journal of the Atmospheric Sciences*, *74*(12), 3891–3900. https://doi.org/10.1175/JAS-D-17-0102.1

Rouault, M. (2003). *Southeast Atlantic warm events and southern African rainfall*. Paper presented at EGS-AGU-EUG Joint Assembly.

Salamalikis, V., Argiriou, A., & Dotsika, E. (2016). Isotopic modeling of the sub-cloud evaporation effect in precipitation. *Science of the Total Environment*, *544*, 1059–1072. https://doi.org/10.1016/j.scitotenv.2015.11.072

Sánchez-Murillo, R., Birkel, C., Welsh, K., Esquivel-Hernández, G., Corrales-Salazar, J., Boll, J., et al. (2016). Key drivers controlling stable isotope variations in daily precipitation of Costa Rica: Caribbean Sea versus Eastern Pacific Ocean moisture sources. *Quaternary Science Reviews*, *131*, 250–261. https://doi.org/10.1016/j.quascirev.2015.08.028

Sánchez-Murillo, R., Durán-Quesada, A. M., Birkel, C., Esquivel-Hernández, G., & Boll, J. (2017). Tropical precipitation anomalies and d-excess evolution during El Niño 2014-16. *Hydrological Processes*, *31*(4), 956–967. https://doi.org/10.1002/hyp.11088

Schmidt, G. A., Hoffmann, G., Shindell, D. T., & Hu, Y. (2005). Modeling atmospheric stable water isotopes and the potential for constraining cloud processes and stratosphere-troposphere water exchange. *Journal of Geophysical Research*, *110*, D21314. https://doi.org/10.1029/2005JD005790

Schumacher, C., & Houze, R. A. Jr. (2003). Stratiform rain in the tropics as seen by the TRMM precipitation radar*. *Journal of Climate*, *16*(11), 1739–1756. https://doi.org/10.1175/1520-0442(2003)016<1739:SRITTA>2.0.CO;2

Shie, C.-L., Tao, W.-K., & Simpson, J. (2006). A note on the relationship between temperature and water vapor over oceans, including sea surface temperature effects. *Advances in Atmospheric Sciences*, *23*(1), 141–148. https://doi.org/10.1007/s00376-006-0014-5

Sinclair, K., Marshall, S., & Moran, T. (2011). A Lagrangian approach to modelling stable isotopes in precipitation over mountainous terrain. *Hydrological Processes*, *25*(16), 2481–2491. https://doi.org/10.1002/hyp.7973

Sjostrom, D. J., & Welker, J. M. (2009). The influence of air mass source on the seasonal isotopic composition of precipitation, eastern USA. *Journal of Geochemical Exploration*, *102*(3), 103–112. https://doi.org/10.1016/j.gexplo.2009.03.001

Soderberg, K., Good, S. P., O'Connor, M., Wang, L., Ryan, K., & Caylor, K. K. (2013). Using atmospheric trajectories to model the isotopic composition of rainfall in central Kenya. *Ecosphere*, *4*, 1–18.

Stein, A., Draxler, R., Rolph, G., Stunder, B., Cohen, M., & Ngan, F. (2015). NOAA's HYSPLIT atmospheric transport and dispersion modeling system. *Bulletin of the American Meteorological Society*, *96*(12), 2059–2077. https://doi.org/10.1175/BAMS-D-14-00110.1

Steiner, M., & Smith, J. A. (1998). Convective versus stratiform rainfall: An ice-microphysical and kinematic conceptual model. *Atmospheric Research*, *47*, 317–326.

Stewart, M. K. (1975). Stable isotope fractionation due to evaporation and isotopic exchange of falling waterdrops: Applications to atmospheric processes and evaporation of lakes. *Journal of Geophysical Research*, *80*, 1133–1146. https://doi.org/10.1029/JC080i009p01133

Stumpp, C., Klaus, J., & Stichler, W. (2014). Analysis of long-term stable isotopic composition in German precipitation. *Journal of Hydrology*, *517*, 351–361. https://doi.org/10.1016/j.jhydrol.2014.05.034

Sturm, C., Zhang, Q., & Noone, D. (2010). An introduction to stable water isotopes in climate models: Benefits of forward proxy modelling for paleoclimatology. *Climate of the Past*, *6*(1), 115–129. https://doi.org/10.5194/cp-6-115-2010

Sturm, M., Zimmermann, M., Schütz, K., Urban, W., & Hartung, H. (2009). Rainwater harvesting as an alternative water resource in rural sites in central northern Namibia. *Physics and Chemistry of the Earth, Parts A/B/C*, *34*(13-16), 776–785. https://doi.org/10.1016/j.pce.2009.07.004

Terzer, S., Wassenaar, L., Araguás-Araguás, L., & Aggarwal, P. (2013). Global isoscapes for δ 18 O and δ 2 H in precipitation: Improved prediction using regionalized climatic regression models. *Hydrology and Earth System Sciences*, *17*(11), 4713–4728. https://doi.org/10.5194/hess-17-4713-2013

Tian, C., Wang, L., Kaseke, K. F., & Bird, B. W. (2018). Stable isotope compositions (δ^2H, δ^{18}O and δ^{17}O) of rainfall and snowfall in the central United States. *Scientific Reports*, *8*(1), 6712. https://doi.org/10.1038/s41598-018-25102-7

Tian, C., Wang, L., & Novick, K. A. (2016). Water vapor δ^2H, δ^{18}O and δ^{17}O measurements using an off-axis integrated cavity output spectrometer—Sensitivity to water vapor concentration, delta value and averaging-time. *Rapid Communications in Mass Spectrometry*, *30*(19), 2077–2086. https://doi.org/10.1002/rcm.7714

Treble, P., Budd, W., Hope, P., & Rustomji, P. (2005). Synoptic-scale climate patterns associated with rainfall δ 18 O in southern Australia. *Journal of Hydrology*, *302*(1-4), 270–282. https://doi.org/10.1016/j.jhydrol.2004.07.003

Trenberth, K. E. (1998). Atmospheric moisture residence times and cycling: Implications for rainfall rates and climate change. *Climatic Change*, *39*(4), 667–694. https://doi.org/10.1023/A:1005319109110

Victoria, R. L., Martinelli, L. A., Mortatti, J., & Richey, J. (1991). Mechanisms of water recycling in the Amazon basin: Isotopic insights. *Ambio*, 384–387.

Vimeux, F., Gallaire, R., Bony, S., Hoffmann, G., & Chiang, J. C. (2005). What are the climate controls on δD in precipitation in the Zongo Valley (Bolivia)? Implications for the Illimani ice core interpretation. *Earth and Planetary Science Letters*, *240*(2), 205–220. https://doi.org/10.1016/j.epsl.2005.09.031

Vuille, M., Bradley, R. S., Werner, M., Healy, R., & Keimig, F. (2003). Modeling δ18O in precipitation over the tropical Americas: 1. Interannual variability and climatic controls. *Journal of Geophysical Research*, *108*(D6), 4174. https://doi.org/10.1029/2001JD002038

Wang, L., Caylor, K., & Dragoni, D. (2009). On the calibration of continuous, high-precision $\delta^{18}O$ and $\delta^{2}H$ measurements using an off-axis integrated cavity output spectrometer. *Rapid Communications in Mass Spectrometry*, *23*(4), 530–536. https://doi.org/10.1002/rcm.3905

Wang, S., Zhang, M., Che, Y., Zhu, X., & Liu, X. (2016). Influence of below-cloud evaporation on deuterium excess in precipitation of arid central Asia and its meteorological controls. *Journal of Hydrometeorology*, *17*(7), 1973–1984. https://doi.org/10.1175/JHM-D-15-0203.1

Welp, L. R., Lee, X., Griffis, T. J., Wen, X.-F., Xiao, W., Li, S., et al. (2012). A meta-analysis of water vapor deuterium-excess in the midlatitude atmospheric surface layer. *Global Biogeochemical Cycles*, *26*, GB3021. https://doi.org/10.1029/2011GB004246

Werner, M., Langebroek, P. M., Carlsen, T., Herold, M., & Lohmann, G. (2011). Stable water isotopes in the ECHAM5 general circulation model: Toward high-resolution isotope modeling on a global scale. *Journal of Geophysical Research*, *116*, D15109. https://doi.org/10.1029/2011JD015681

Wu, H., Zhang, X., Xiaoyan, L., Li, G., & Huang, Y. (2015). Seasonal variations of deuterium and oxygen-18 isotopes and their response to moisture source for precipitation events in the subtropical monsoon region. *Hydrological Processes*, *29*(1), 90–102. https://doi.org/10.1002/hyp.10132

Yurtsever, Y. (1975). Worldwide survey of stable isotopes I precipitation, *Rep. Sect. Isotope Hydrol., IAEA*.

Zhao, L., Wang, L., Liu, X., Xiao, H., Ruan, Y., & Zhou, M. (2014). The patterns and implications of diurnal variations in the d-excess of plant water, shallow soil water and air moisture. *Hydrology and Earth System Sciences*, *18*(10), 4129–4151. https://doi.org/10.5194/hess-18-4129-2014

Zhao, L., Xiao, H., Zhou, M., Cheng, G., Wang, L., Yin, L., & Ren, J. (2012). Factors controlling spatial and seasonal distributions of precipitation $\delta^{18}O$ in China. *Hydrological Processes*, *26*(1), 143–152. https://doi.org/10.1002/hyp.8118